1
Nanoparticle- and Nanofiber-Based Polymer Nanocomposites: An Overview

Muthukumaraswamy Rangaraj Vengatesan and Vikas Mittal

1.1
Introduction

Polymer nanocomposites are three-dimensional (3-D) materials generated by the combination of polymer matrix with different reinforcement materials, in which at least one of the filler dimensions is on the nanoscale level [1–3]. Generally, zero-dimensional (0-D), one-dimensional (1-D), two-dimensional (2-D), and 3-D nanomaterials are used as filler materials for the fabrication of polymer nanocomposites. Nanoscale materials possess a large surface area for a given volume [4–7]. It is also well known that the high aspect ratio of nanomaterials (especially fibers) provides superior nanoreinforcement effect on polymer nanocomposites properties. Predictably, the properties of polymer nanocomposites are significantly influenced by the size of the nanomaterial and the quality of interface between the matrix material and the filler material [8]. The nanomaterials can interact chemically or physically with polymer interfaces, thus, resulting in nanocomposites with superior properties compared to virgin polymer. As a result, the incorporation of even low weight percent of filler is observed to improve the mechanical properties, thermal stability, heat distortion temperature, chemical resistance, electrical conductivity, and optical clarity of the parent polymer systems significantly. The polymer nanocomposites are ideal candidate materials in many applications, including aerospace applications, automobile manufacturing, biomedical, coatings, and sensors [9]. Different types of nanoparticles and nanofibers have been employed in the literature to develop the polymer nanocomposites.

This review is focused on the fundamental synthetic methods and effect of the nanofillers such as spherical nanoparticles and nanofibers on the properties of the polymer matrices. The applications of nanoparticle- and nanofiber-based nanocomposites have also been summarized and discussed.

Spherical and Fibrous Filler Composites, First Edition. Edited by Vikas Mittal.

1.2 Nanoparticles

Nanoparticles (NPs) with sizes of 5–100 nm have gained significant attention from the perspective of both academic and industrial use in a wide range of applications (Figure 1.1) [10]. This study focuses on such nanoparticles in zero-dimensional (0-D) architecture with controllable size. A variety of metals and metal oxides have been adopted to fabricate the nanoparticles within a nanoscale level, for example, core–shell nanoparticles and nanodots. These nanoparticles exhibit the size- and surface-area-controllable properties such as optical, magnetic, electrical, and catalytic. These properties lead to the use of nanoparticles in different areas such as optical, biomedical, and sensors [11].

1.2.1 Synthesis of Nanoparticles

Different physical and chemical routes have been used to prepare the nanoparticles such as the following:

1) *Physical methods*
   a. Thermal decomposition [12–15]

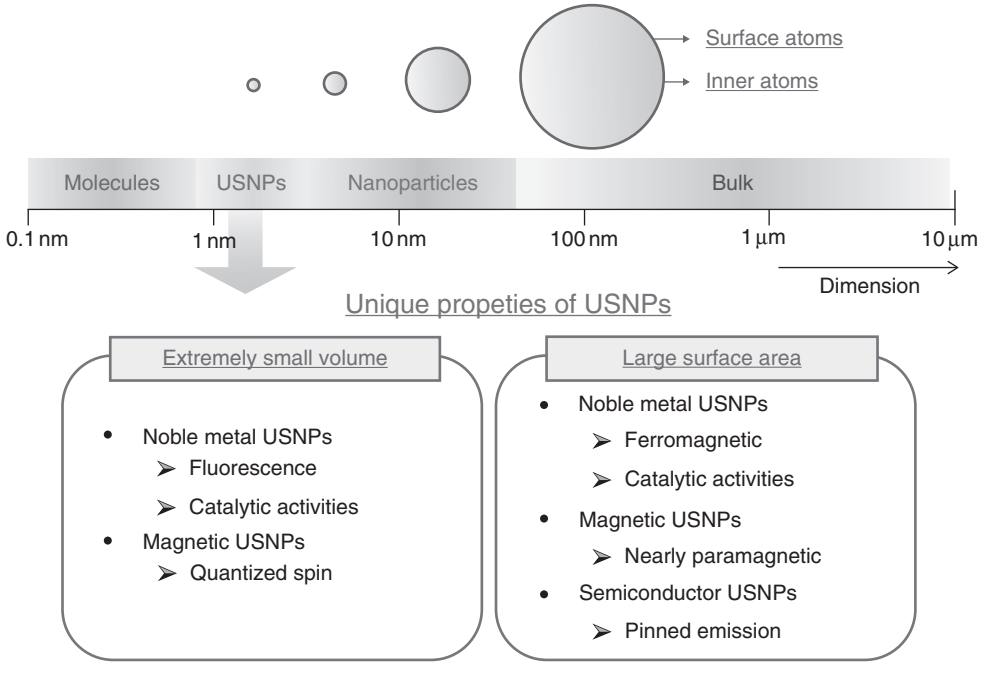

Figure 1.1 Schematic representation of differences in the sizes of particles and their resultant properties. (Kim *et al.* [10]. Reproduced with permission of American Chemical Society.)

b. Ball milling [16–18]
c. Spray pyrolysis [19–21].

2) *Chemical methods*
a. Sol–gel synthesis [22–24]
b. Precipitation [25, 26]
c. Hydrothermal [27–29]
d. Solvothermal [30–32].

1.3 Fibrous Nanomaterials

Fibrous nanomaterials consist of both nanofibers and nanowires in one-dimensional (1D) architecture with unique properties. These materials exhibit high surface area and porosity with a diameter ranging from 50 to 500 nm. Different types of fibrous materials are available such as naturally occurring nanofibers (natural sepiolite clay fibers, cellulose fibers, sisal fibers, etc.), carbon fibers (CFs), metal nanofibers/wires (silver (Ag) nanowires, gold (Au) nanowires, etc.), metal-oxide-based fibers (zinc oxide (ZnO) nanofibers, titanium dioxide (TiO_2) nanofibers and wires, silica (SiO_2) nanofibers, cerium dioxide (CeO_2) nanofibers, copper oxide (CuO) nanowires, etc.), bionanofibers, and polymer nanofibers. Fibrous nanomaterials have been widely used in multiple applications such as composites, microelectronics, biosensors, sensors, biomedical, and coatings. Apart from the natural fibers, several approaches have been used to fabricate the fibrous nanomaterials. Among these, self-assembling and electrospinning techniques have been widely used for the preparation of nanofibers.

1.3.1 Self-Assembly Method

Self-assembly is one of the common techniques used to prepare fibrous nanomaterials via intermolecular noncovalent interactions, such as van der Waals forces, hydrogen bonding, and ionic and coordinative interactions [33]. The nanofibrous materials are prepared in different physiochemical conditions such as solvothermal, hydrothermal via self-assembling mechanism. In this method, ionic liquids, biomolecules, surfactants, and block copolymers have been used as soft templates to prepare the nanofibers/wires. Jian *et al.* prepared Ag nanowires with a diameter in the range of 15–25 nm [34]. The Ag nanowires were grown in the presence of gemini surfactant 1,3-bis(cetyldimethylammonium) propane dibromide via solvothermal method [34]. Song *et al.* synthesized platinum nanowire networks by chemical reduction of a platinum complex using sodium borohydride in the presence of cetyltrimethylammonium bromide (CTAB)in a two-phase water–chloroform system as the soft template [35]. Chang *et al.* prepared thin and long Ag nanowires in the presence of ionic liquids, tetrapropylammonium chloride, and tetrapropylammonium bromide with a diameter of

40–50 nm. This method has been widely utilized for the fabrication of bio-based nanofibers in biomedical applications [36]. Zhou *et al.* synthesized net-like ZnO nanofibers via a surfactant-assisted hydrothermal method. The nanofibers were grown in the presence of polyethylene glycol (PEG) via self-assembling method [37]. Charbonneau *et al.* (2012) developed rutile TiO_2 nanofibers via controlled forced hydrolysis of titanium tetrachloride solution [38]. Dong *et al*. [39] synthesized zirconium dioxide (ZrO_2) nanowires via the solvothermal reaction of zirconium tetra-*n*-propoxide Zr (OPrn) with ethylene glycol and 1-butyl-3-methyl imidazolium tetrafluoroborate ionic liquid at 160 °C [40]. Polymer nanofibers have been synthesized via self-assembling of block copolymers. The nanofibers exhibited a diameter of approximately 80 nm and the length was in the range of several hundred nanometers. These polymer nanofibers were used as template materials for the fabrication of carbon nanofibers (CNFs) (Figure 1.2) [41, 42]. Conducting metal wires have been prepared using bimolecular template via self-assembling method [43].

1.3.2 Electrospinning Method

Electrospinning is one of the most versatile processes for fabricating nanofibers. A variety of fibrous (fibers/wires) nanomaterials such as metals, metal oxides, polymers, and carbon have been fabricated using this method. The other physical methods such as hydrothermal and solvothermal have certain limitations for the large-scale production and uniform size of nanomaterials. However, electrospinning is a facile process to produce various nanofibers at larger scales. In this process, polymer solution or precursor of metal or metal oxide solution is filled in a pipette, which is held in between the two electrodes containing DC voltage supply in the kilovolts range. The repulsive force of the precursor solution should be higher than its surface tension. The solution drops from the tip of the pipette with high voltage, thus, generating a fibrous material. The size of the fibrous material mainly depends on the parameters such as solution viscosity, conductivity, applied voltage, spinneret tip-to-collector distance, and humidity. The electrospinning technology is widely used to prepare the polymer composite fiber material [44]. Shao *et al.* developed poly(vinyl alcohol) (PVA)/silica (SiO_2) composite thin fibers in the diameter of 200–400 nm via electrospinning method [45]. Dong *et al.* prepared polyvinylidene fluoride (PVDF)-SiO_2 composite nanofiber membrane via electrospinning method [46]. Bae *et al.* fabricated porous poly(methyl methacrylate) (PMMA) nanofibers via electrospinning technique using a binary solvent system (8 : 2 dichloromethane: dimethylformamide) under controlled humidity (Figure 1.3) [47]. A number of electrospun polymer nanofibers have been utilized as template materials for the preparation of carbon, metal, and metal oxide nanofibrous materials. Polyacrylonitrile (PAN) is a widely used polymer precursor for the preparation of CNFs via electrospinning method. Gu *et al.* prepared PAN nanofibers as precursors of CNFs with diameters in the range of 130–280 nm through electrospinning

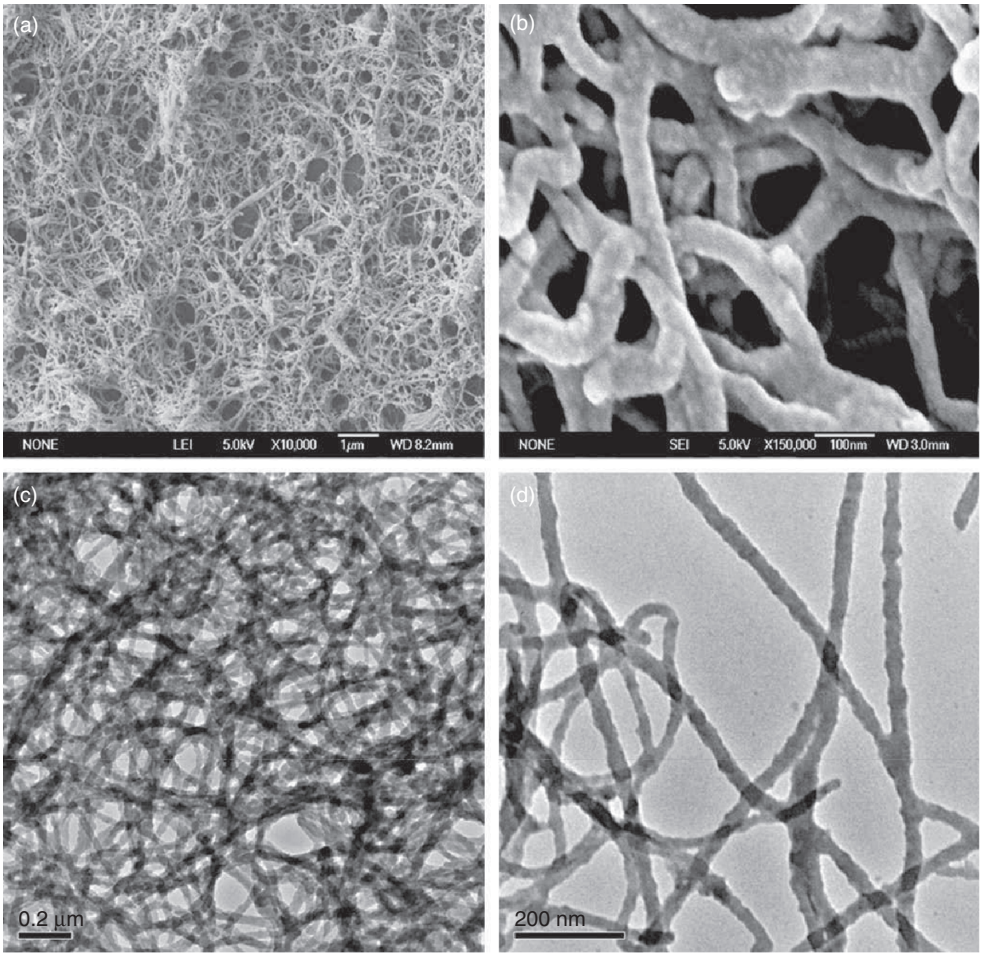

Figure 1.2 (a,b) Field-emission SEM images of the poly (cyclotriphosphazene-4,4′sulfonyldiphenol) (PZS) nanofibers. (c,d) HR-TEM images of the PZS nanofibers. (Fu *et al.* [41]. Reproduced with permission of Elsevier.)

method [48]. Zhou *et al.* developed aligned CFs from the aligned PAN fibers via electrospinning method. The aligned CFs exhibited anisotropic electrical conductivities and good mechanical properties [49]. Park *et al.* fabricated hollow ZnO nanofibers from the electrospun polymer. The ZnO precursor deposited on the electrospun polymer and subsequent heat treatment resulted in the selective removal of the polymer template and the formation of hollow ZnO nanofibers [50]. Liu *et al.* fabricated TiO_2 nanofibers with diameter ranging 600–700 nm via electrospinning technique using polylactic acid (PLA), tetrabutyl titanate, and hexafluoroisopropanol as a spinning solution [51]. Metal nanofibers/wires have been prepared by this method for use in microelectronics application. Wu *et al.* developed high-performance transparent electrodes with copper (Cu) nanofiber

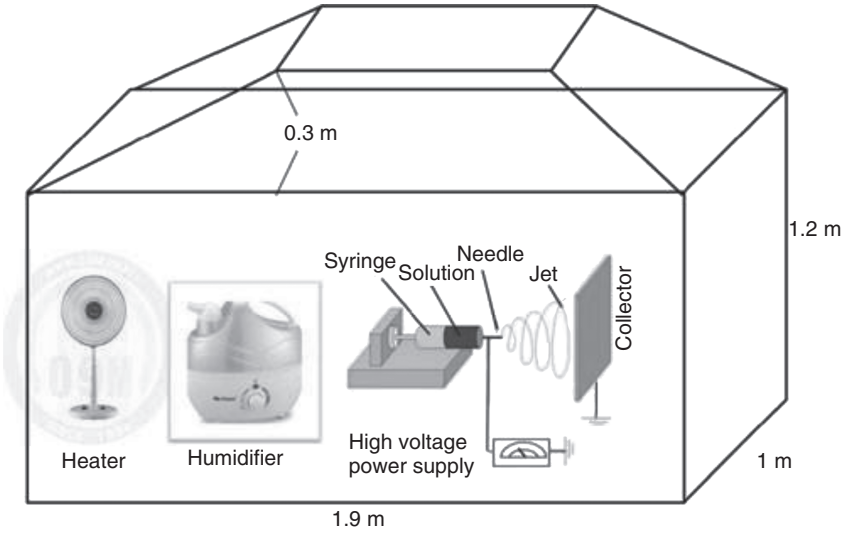

Figure 1.3 Schematic representation of electrospinning chamber. (Bae *et al.* [47]. Reproduced with permission of Springer Publishing Company.)

networks by a low-cost and scalable electrospinning process. The Cu nanofibers exhibited high transmittance with low shear rate [52]. Gries *et al.* prepared gold nanowires (AuNWs) using highly concentrated aqueous dispersions of gold nanoparticles (AuNPs) by the electrospinning method in the presence of PVA and subsequent annealing at higher temperature [53].

1.3.3 Miscellaneous Methods

1.3.3.1 Chemical Vapor Deposition Method (CVD)

1-D fibrous nanomaterials have also been synthesized via vapor phase method. In this method, vapor species are generated from the precursor via evaporation, chemical reduction, and gaseous reaction steps. Subsequently, the generated vapor species are condensed on the solid surface. Generally, the vapor-phase synthesis process is carried out at higher temperatures from 500 to 1500 °C and produces high-quality nanowires [54]. A variety of methods are involved in the preparation of nanowires on vapor-phase level. Among these, chemical vapor deposition (CVD) is one of the techniques to fabricate the fibrous material on nanoscale level. Chang *et al.* synthesized ZnO nanowires via modified CVD method (Figure 1.4) [55]. CNFs have been synthesized in high yields (>70%) by CVD method in the presence of Co/LiF catalyst using acetylene as the carbon source [56]. Fu *et al.* prepared large quantities of silicon carbide (SiC) nanowires using CH_3SiCl_3 (methyl trichlorosilane (MTS)) and H_2 as the precursors by CVD method. The SiC nanowires exhibited a single-crystal β-SiC structure, with diameters of about 70 nm [57].

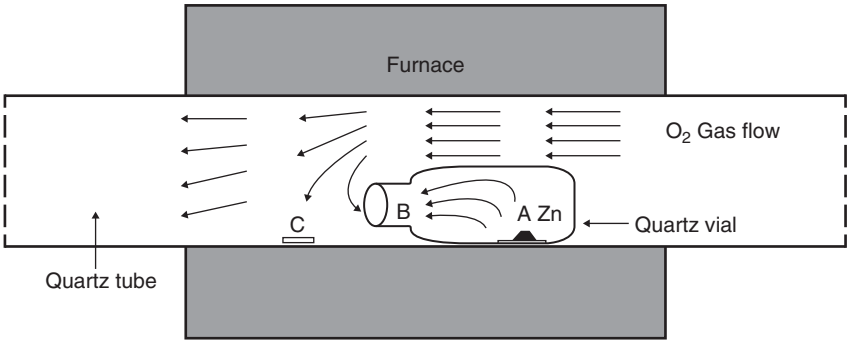

Figure 1.4 Schematic representation of the CVD system with a horizontal quartz tube placed in a furnace. A small quartz vial inside the quartz tube is used to trap zinc vapor during the synthesis process. (Chang *et al.* [55]. Reproduced with permission of American Chemical Society.)

1.3.3.2 **Thermal Evaporation**

Thermal evaporation is one of the physical deposition methods and is widely used to fabricate 1-D nanomaterials. The thermal evaporation process is more facile, flexible, and cheap. Many metal oxide fibrous nanomaterials have been synthesized using this method. For example, SnO_2, TiO_2, indium oxide (In_2O_3), ZnO, and SiO_2 nanowires have been prepared by this method [58–62].

1.4 Nanoparticle-Reinforced Polymer Nanocomposites

The molecular-level uniform dispersion of nanoparticles can lead to a large interfacial area in the polymer nanocomposites. Therefore, the strong interfacial interaction between the organic and inorganic phases creates a high impact on the properties of the polymer nanocomposites. A variety of nanoparticles have been utilized for the development of polymer nanocomposites, which result in materials with improved electrical, rheological, and tribological properties.

1.4.1 Effect of Size and Dispersion of Nanoparticles in Polymer Matrices

The size and dispersion of the nanoparticles are important criteria for the reinforcement effect of the polymer nanocomposites. The size of nanoparticles affects the polymer dimensions in nanocomposites for the cases when the polymer radius of gyration (R_g) is larger or of the order of the nanoparticle radius (R). The quality of nanoparticle dispersion can have an important effect on the polymer chain dimensions, and this depends on the nanoparticle–polymer interactions, nanoparticle–polymer size ratio, size of nanoparticles, and nanoparticle volume fraction [63–65]. Recently, Karatrantos *et al.* investigated the effect of

various spherical nanoparticles on chain dimensions in polymer melts for high nanoparticle loading, which was larger than the percolation threshold, using molecular dynamics simulations. The authors observed that the entanglement length decreases significantly with the volume fraction of nanoparticles. The addition of nanoparticles in the polymer matrix increases the counter path of the primitive path [66, 67]. The nanoparticles with a uniform size behave as highly isotropic materials; therefore, these can easily bind with the polymer matrix in melt state condition and can be easily processed via extrusion and injection molding. In addition, the nature of the nanoparticles (hydrophobic or hydrophilic) is the important phenomenon for the uniform dispersion in the polymer matrix. In general, most of nanoparticles are polar as well as hydrophilic and are incompatible with organic polymer matrices. In order to improve the dispersibility, the nanoparticles are further modified using surface functionalization methods [68]. Obviously, the nanoparticle feed ratio also influences the properties of the polymer matrix. The incorporation of volume fraction of nanoparticles in the polymer matrix has some threshold level, and above that level, it creates agglomeration in polymer nanocomposites, resulting in a reduction of polymer properties [69].

1.4.2 Influence of Nanoparticles on the Thermal Properties of Polymer Nanocomposites

The loading amount of the nanoparticles is an important parameter for the thermal properties of the polymer matrix. The surface modification of the nanoparticle is also an important factor for improving the interfacial adhesion between the nanoparticle and polymer matrices. An equal amount of surface-modified nanoparticles possess high degree of dispersion in the polymer matrix compared to unmodified nanoparticles dispersed in the polymer matrix. Hamming *et al.* studied the quality of dispersion and interfacial interaction between TiO_2 nanoparticles and host polymer, along with the effect on glass transition temperature (T_g). The authors observed that the bulk properties of nanocomposites are highly sensitive to both the quality of the interfacial interaction and quality of dispersion of the nanoparticles and that these factors must be controlled to create the nanocomposites with specific and predictable behavior [70]. Mandhakini *et al.* studied the tribological properties of epoxy nanocomposites with the addition of different weight ratios of alumina nanoparticles. The authors observed that the addition of alumina content from 1 to 5 wt% increases the T_g of the polymer nanocomposites, which is attributed to decrease in the polymer–polymer interface and restricted chain mobility of polymer segments resulting from good adhesion between the nanoparticles and the surrounding polymer matrix. At a higher loading (10 wt%), a decrease in T_g was observed [71]. Rajamanikam *et al.* (2015) studied optical and thermomechanical behavior of benzoxazine functionalized ZnO-reinforced polybenzoxazine nanocomposites. The authors observed that the surface modification of ZnO strongly improves the interfacial adhesion with the polymer matrix. The higher loading of 10 wt% ZnO

exhibited higher T_g compared to pure polymer matrix [72]. The incorporation of nanoparticles in semicrystalline polymers tends to increase the rate of crystallization, which results in higher crystallinity, higher crystallization temperature, and smaller spherulites. The addition of nanoparticles induces the other forms of polymer crystalline phase due to the nucleation effect in the polymer matrix. For example, spherical calcium carbonate induces the β phase of the polypropylene (PP) and also increases crystallinity [73, 74]. Farhoodi *et al.* investigated the effect of TiO_2 on the physical properties of polyethylene terephthalate (PET) nanocomposites. The authors concluded that the addition of nanoparticle increases the crystallinity of PET up to 3 wt% and higher loading results in decrease in crystallinity due to the agglomeration of the nanoparticles [75]. Yu *et al.* studied the influence of ZnO nanoparticles on the crystallization behavior of electrospun poly(3-hydroxybutyrate-*co*-3-hydroxyvalerate) (PHBV) nanofibers. The authors observed decrease in crystallinity of PHBV with the addition of ZnO. This is due to the interaction of hydrogen bonds between ZnO NPs and PHBV, which hinders the crystallization at lower temperatures (Figure 1.5) [76]. The size of the nanoparticle influences the thermal stability of the polymer matrix. Gomez *et al.* developed PP nanocomposites using silica nanoparticles with 20–100 nm diameter. The authors concluded that the nanoparticles improved the thermal stability of PP through the adsorption of volatile compounds on the surface, where the smaller nanoparticles show the greatest stabilization [77]. Jin *et al.* developed epoxy nanocomposites with SiO_2 nanoparticles. The authors observed that the addition of SiO_2 nanoparticle improved the thermal stability of epoxy by 30% [78]. Isitman *et al.* studied the role of nanoparticle geometry in flame retardancy of polylactide nanocomposites containing aluminum phosphinate. Two-dimensional (2-D) nanomaterials possess better flame-retardant property compared to 0-D and 1-D nanomaterials [79].

1.4.3
Influence of Nanoparticles on the Mechanical Properties of Polymers

The nanoparticle size, particle–matrix interface adhesion, and loading amount strongly influence the mechanical properties of nanoparticle-reinforced polymer composites. The nanoparticles readily enhance Young's modulus of polymer matrices, which is due to higher stiffness of nanoparticles as compared to pure polymer. The stress transfer mechanism plays an important role in the nanoparticle-reinforced polymer nanocomposites. The strength of the polymer nanocomposites mainly depends on the stress transfer between the polymer matrix and the nanoparticles. The strong interfacial adhesion effectively improves the stress transfer mechanism from particles to polymer matrix, resulting in an increase in strength of the polymer nanocomposites [80]. Many studies have shown that the rigid nanoparticles improved the fracture toughness of the thermoset polymers compared to thermoplastics; however, in contrast, the rigid calcium carbonate particles have been reported to enhance the fracture toughness of the PP [81, 82] and high-density polyethylene (HDPE) [83–85]. As the strong

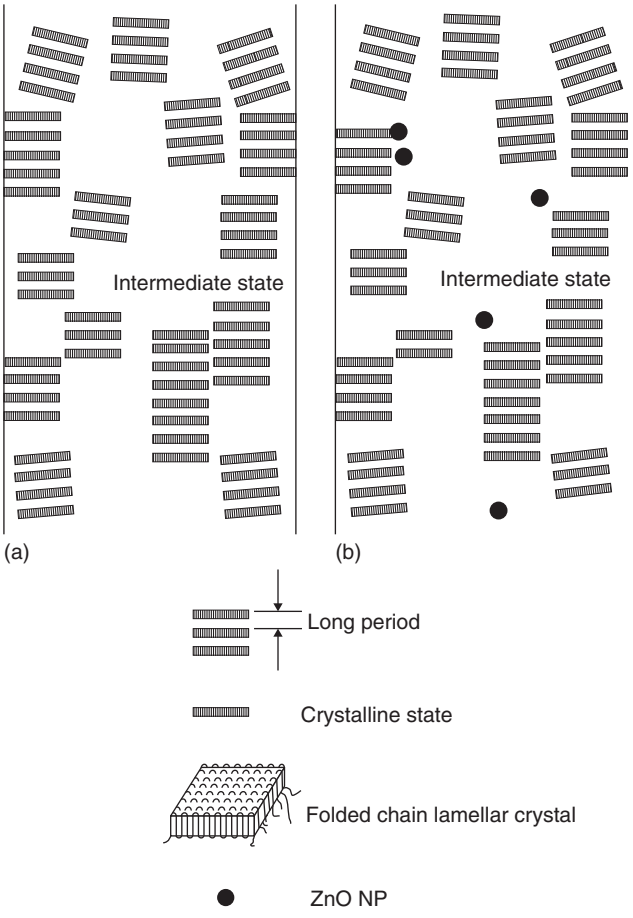

Figure 1.5 Schematic representation of (a) pure PHBV and (b) composite ZnO NPs/PHBV fiber. (Yu *et al.* [76]. Reproduced with permission of Elsevier.)

interfacial adhesion mechanism strongly improves the mechanical properties of the nanocomposites, thus, in order to achieve better interfacial adhesion, the surface of the nanoparticles needs to be modified with suitable coupling agents. Hussain *et al.* studied the effects of different coupling agents on the mechanical properties of the TiO_2-particles-filled epoxy nanocomposites. It was observed that the titanate coupling agent treated TiO_2 nanoparticles significantly improved Young's modulus and flexural strength of the epoxy composites compared to silane coupling agent treated TiO_2 nanoparticles [86]. Yoshida *et al.* studied the effect of silane coupling agent on tensile and bending properties of silica-filled epoxy nanocomposites. The authors observed that the silane coupling agents improved the adhesion between epoxy resin and SiO_2 nanoparticles in composite [87]. Ash *et al.* synthesized and studied the mechanical behavior of PMMA/Al_2O_3 nanocomposites using 38- and 17-nm-sized alumina nanoparticles. The authors

observed a weak interface between the nanoparticles and polymer, which leads to brittle-to-ductile transition at room temperature. They also found that the brittle-to-ductile transition requires both the enhanced polymer chain mobility attributed to smaller particles and the ability to release the stress triaxiality by poorly bonded larger particles [88]. Jeziórska *et al.* developed low-density polyethylene (LDPE)/SiO_2 nanocomposites via melt extrusion method and studied the mechanical properties of the composites with the effect of silica size, functionality, and compatibilizer. It was observed that the addition of modified silica and glycidyl-methacrylate-grafted ethylene/*n*-octene copolymer (EOR-g-GMA) enhanced the tensile strength, modulus, and impact strength due to better dispersion of SiO_2 nanoparticles and increased compatibility between silica and the LDPE matrix [89]. Rao *et al.* studied the mechanical properties of copper oxide (CuO)-nanoparticles-filled PVA nanocomposites. The elastic modulus and toughness of the nanocomposites increased linearly up to lower wt% of CuO nanoparticles (2 wt%), whereas the higher content of CuO exhibited decrease in the mechanical properties of PVA due to the agglomeration [90]. Rithin Kumar *et al.* developed PVA composite films using ZnO and tungsten trioxide (WO_3) nanoparticles via solution casting method and observed that the addition of ZnO and WO_3 increased the tensile strength and Young's modulus up to 14 wt% [91]. Salehian and Jahromi studied the mechanical properties of vinyl-ester-based nanocomposites with effect of different weight ratio of TiO_2 nanoparticles. They observed that the addition of small fraction of nanoparticles increased the mechanical properties of vinyl ester composites [92]. Liawthanyarat and Rimdusit developed polybenzoxazine nanocomposites with different-sized silica nanoparticles in fixed weight ratio (3 wt%). The authors observed that the small size of silica nanoparticles systematically increased the storage modulus of the polybenzoxazine nanocomposite and also resulted in greater barrier effect due to the larger surface area of the smaller particles [93].

1.4.4
Electrical Properties of Nanoparticle-Reinforced Polymer Nanocomposites

Polymer nanocomposites with metal, metal oxides, carbon nanoparticles as reinforcements are widely used to fabricate the advanced devices in electronic and optoelectronic applications. The addition of metal and metal oxide nanoparticles in the polymer matrices has gained a considerable attention due to their enhanced electrical properties [66]. Similar to the mechanical properties, the fundamental electrical properties of the polymer nanocomposites have been studied with effects of size, shape, and loading concentration of the fillers [94, 95]. The improvement of dielectric properties of nanocomposites mainly depends on the (i) the large surface area of nanoparticles, which creates large interaction with the polymer matrix; (ii) changing the polymer morphology due to the surface of nanoparticles; (iii) size effect; (iv) charge distribution between the nanoparticles and the matrix; and (v) scattering effect [67, 69]. The interface between the polymer and the particles has an important role in

varying the dielectric properties of the nanocomposites. The large interfacial interaction between the nanoparticles and polymer matrix leads to improved dielectric properties of the nanocomposites. It is well known that the metal oxide nanoparticles possess high surface energy. The unmodified nanoparticles can create agglomeration in the composites, which results in reduced dielectric properties. Thus, to improve dispersion of nanoparticles, the surface modification of nanoparticles has been achieved with suitable coupling agents [96]. Zhaa *et al.* developed polyimide (PI)-TiO_2 nanocomposite film via *in situ* polymerization process. The authors studied the dielectric permittivity of composite films with the effect of frequency, temperature, and the nano-TiO_2 particles loading concentration. It was observed that the interfacial polarization existed in the PI/TiO_2 nanocomposite films with different loading concentrations of the nano-TiO_2 particles (Figure 1.6) [97]. Tuncer *et al.* studied the electrical properties of epoxy nanocomposites with barium titanate ($BaTiO_3$) and calcium copper titanate ($CaCu_3Ti_4O_{12}$) nanoparticles. The addition of nanoparticles decreased

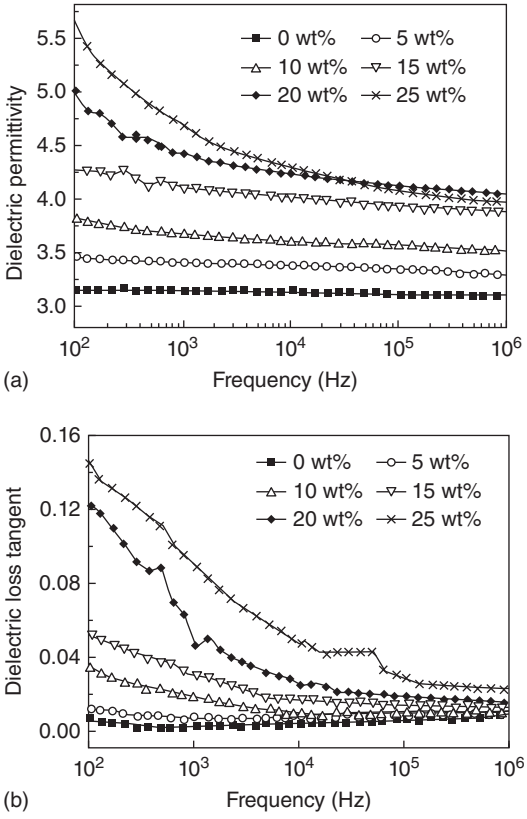

Figure 1.6 Dependence of (a) dielectric permittivity and (b) dielectric loss tangent of the PI/TiO_2 nanocomposite films on the concentration of nano-TiO_2 particles. (Zhaa *et al.* [97]. Reproduced with permission of Elsevier.)

the breakdown strength of the matrix resin significantly [98]. Jaing *et al.* studied the dielectric properties of epoxy nanocomposites with two different sizes of surface-modified SiO_2 nanoparticles such as 20 and 100 nm. The incorporation of 20-nm surface-modified SiO_2 nanoparticles resulted in high dielectric constant with low dielectric loss compared to the 100 nm surface-modified SiO_2 nanoparticles [99]. Yang *et al.* prepared styrene-*b*-ethylene/butylene-*b*-styrene (SEBS)–iron(III) oxide (Fe_3O_4) nanocomposites and studied the effect of size of magnetic nanoparticles on the resultant magnetodielectric properties of polymer nanocomposites at radio frequencies. The dielectric permittivity of the polymer composite increased with increasing amount of loading amount of Fe_3O_4, but not with the size of nanoparticles. However, the magnetic permeability of the composites was significantly influenced by the size of Fe_3O_4 nanoparticles due to thermal energy fluctuations from the nanoparticle surroundings [100]. Chandrakala *et al.* developed PVA composite films using ZnO-Ce_2O_3 nanoparticles and studied the electrical properties. The dielectric constant and dielectric loss of the nanocomposites increased with increase in nanoparticle concentration, but decreased with increase in frequency. It was concluded that the AC conductivity of PVA/ZnO-Ce_2O_3 nanocomposites increased with increasing frequency [101]. Hong *et al.* studied the rescaled electrical properties of ZnO/LDPE nanocomposites. The composites exhibited slow decrease in DC resistivity with increase in filler concentration and the breakdown voltage of composite was higher with high content of nanofiller [102]. The incorporation of conducting metal nanoparticles in the polymer matrix enhanced the dielectric constant of the nanocomposite. Goyal and Sulakhe developed PVDF-Ni nanocomposites and studied the electrical conductivity of the nanocomposites. The authors observed that the electrical conductivity of PVDF increased from 6.3×10^{-13} S cm^{-1} to 2.6×10^{-1} S cm^{-1} [103]. Mahendi *et al.* studied the electrical conductivity and dielectric properties of Ag-nanoparticle-filled PVA nanocomposites. With increase in concentration of Ag nanoparticles in PVA from 0 to 1.32 wt%, the DC conductivity of the nanocomposites increased from 1.38×10^{-11} S cm^{-1} to 9.17×10^{-11} S cm^{-1} and decrease in frequency-dependent dielectric constant (from 1.74 to 1.07 at 75 kHz) was observed [104]. The metal-nanoparticle-incorporated nanocomposites have also been used to prepare the electrically conductive adhesives (ECAs) in electronic packaging applications. Tee *et al.* prepared Ag-nanoparticle-filled epoxy composites and studied the electrical and flexural properties. The authors observed that the insulator-to-conductor transition occurred in the nanocomposites with a percolation threshold of 5 vol% of Ag [105].

1.4.5 Application of Nanoparticle-Reinforced Polymer Nanocomposites

1.4.5.1 Coatings

Large scientific efforts are devoted to protect the metallic materials from corrosion. Three approaches are normally used for the reduction of corrosion rate

including cathodic protection, anodic protection (passivation), and application of barrier coatings. Among these, organic coatings have been extensively used as barrier coatings to prevent metals from corrosion [106]. The nanocomposite coatings possess a significant efficiency in the corrosion inhibition compared to conventional coatings. Different types of inorganic nanomaterials, such as clay, organoclay, metal oxide nanoparticles and nanotubes, have been used to prepare organic/inorganic hybrid nanocoatings. Many researchers have developed TiO_2-based organic coatings and reported that the TiO_2 nanoparticles have advantages such as good stability, high refractive index, hydrophilicity, ultraviolet (UV) resistance and excellent transparency for the visible light, nontoxicity, high photocatalytic activity, and low cost [106–108]. Shaik *et al.* developed caster-oil-based poly(urethane-etherimide)/TiO_2 coatings. The nanocomposite coatings had good physical, mechanical, anticorrosion, and antimicrobial properties and could be safely used up to 200 °C [109]. Wang *et al.* studied the corrosion performance of waterborne epoxy–TiO_2 hybrid nanocomposite coatings. The electrochemical impedance spectroscopy (EIS) analysis showed that the resistance value of coating with *meso*-TiO_2/poly(etherimide) (PEI) (600 molecular weight) was above 9.87×10^7 cm^2, which was higher than that of neat epoxy coating [110].The other metal and metal oxides such as Ag, SiO_2, Fe_3O_4, and ZnO, have been used as a filler materials for hybrid polymer coatings. Olad and Nosrati [111] developed a coating material using polyvinyl chloride (PVC) and polyaniline-coated ZnO via solution mixing method. PVC/ZnO–polyaniline hybrid nanocomposite coating showed significantly increased corrosion protection effect on iron samples compared to uncoated iron coupon and pure polyaniline anticorrosive coating. Ghanbari and Attar studied the anticorrosion performance of epoxy–silica nanocomposites. EIS and salt spray test results indicated that the incorporation of 4–6 wt% SiO_2 nanoparticles exhibited the best corrosion performance [112].

1.4.5.2 Separation and Purification

Polymer membranes are widely used in separation and purification applications due to their high stability and efficiency, low energy requirements, and easy operation. The major problem with these membranes is fouling, which causes a decline in flux and an increase in the operating cost of the system. In order to resolve this problem, the hydrophilic nanoparticles are incorporated into the polymeric membranes to significantly enhance the pure water flux and the fouling resistance. The size, dispersion, and chemical composition of nanoparticle additives play a major role in determining their effectiveness in improving the membrane properties [113]. Silica, titania, alumina, and ZnO nanoparticles are widely used as filler materials in the ultrafiltration polymer membranes due to high thermal stability and large surface area [114]. Huang *et al.* fabricated polyether sulfone–mesoporous silica (MS) nanocomposite ultrafiltration membranes and studied their antifouling properties. Addition of 2 wt% MS significantly decreased the protein adsorption capacity from 45.8 to 21.4 μg cm^{-2} [115]. Sotto *et al.* studied the antifouling properties of polyethersulfone–TiO_2

composite membranes as a function of TiO_2 doping concentration. Addition of low content of about 0.08 wt% exhibited an optimum permeability and improved the antifouling resistance by about 12% [116]. Maximous *et al.* developed Al_2O_3-doped polyether sulfone membranes for wastewater purification. The addition of alumina nanoparticle lowered the flux decline compared to neat polymeric membrane and also the fouling migration effect increased with the increase in content of alumina (Table 1.1) [117].

The polymer nanocomposite membranes are also widely used for gas separation and removal applications that involve high gas flow rates and high gas concentrations and are advantageous, especially for offshore and remote areas. The membranes are used to separate the acid–gas mixture, for example, H_2S together with CO_2 from gas mixes containing CH_4 based on the solution–diffusion mechanism. The separation and removal performances of these membranes generally depend on the selectivity of H_2S and CO_2 over CH_4, considering that the permeation rates of H_2S and CO_2 are much higher than that of CH_4. The metal-nanoparticle-doped polymer membranes are used in catalytic polymeric membrane reactors (CPMRs). The CPMRs are capable of catalytic reaction with chosen gas species in a single step, producing residues that are inert for the desired system [118]. Nour *et al.* developed Ag-nanoparticle-doped polydimethylsiloxane (PDMS) membrane for H_2S removal. The authors observed that the addition of 1 wt% of Ag nanoparticle in PDMS resulted in more than 60% removal of H_2S gas molecules [118].

1.4.5.3 **Biomedical**

The metal and metal oxide nanoparticles are used as filler materials for the fabrication of biopolymer-based (polysaccharides, aliphatic polyesters, polypeptides and proteins, and polynucleic acids) nanocomposites. The interaction of nanoparticles in the biopolymer matrix at the nanometer scale results in enhanced mechanical properties of the bionanocomposites. Biodegradable polymer nanocomposites are widely used in the biomedical applications such as tissue engineering, bone replacement/repair, dental applications, and controlled drug delivery. Biodegradable polymer nanocomposites are the materials that can degrade and are gradually absorbed and/or eliminated by the body, whether degradation is caused mainly by hydrolysis or mediated by metabolic processes [119]. The polymer nanocomposite for the biomedical application requires

Table 1.1 Filtration resistances of neat and Al_2O_3-doped PES membranes.

Membrane	R_m ($\times 10^7$) (m^{-1})	R_f ($\times 10^7$) (m^{-1})	R_c ($\times 10^7$) (m^{-1})	R_t ($\times 10^7$) (m^{-1})	R_c/R_t (%)
PES	0.34	1.13	6.2	7.6	81.6
0.01 Al_2SO_3/PES	0.38	1.11	0.73	2.22	33
0.03 Al_2SO_3/PES	0.39	0.79	0.61	1.79	34
0.05 Al_2SO_3/PES	0.32	1.16	0.32	1.8	18

Source: Maximous *et al.* [117]. Reproduced with permission of Elsevier.

certain criteria such as biocompatibility, biodegradability, good mechanical properties, and, in some cases, esthetic demands. Therefore, the choices of polymer matrix and nanomaterials are very important for the fabrication of polymer nanocomposites in biomedical applications. Ag and Au nanoparticles are widely used filler materials for the bionanocomposites due to their strong antibacterial property as well as low toxicity. Shameli *et al.* developed Ag-doped polylactic acid (PLA) nanocomposites and studied their antibacterial activity. The authors suggested that Ag/PLA-NC films can be used as an antibacterial scaffold for tissue engineering and medical applications [120]. Carlo *et al.* synthesized Au–chitosan nanocomposites for the caffeic acid sensing application. The authors concluded that the Au–chitosan nanocomposites are sensitive and selective electrochemical sensors for the determination of caffeic acid in a wide range of concentrations from 5.00×10^{-8} to 2.00×10^{-3} M, and the limit of detection (LOD) was estimated to be 2.50×10^{-8} M [121]. Lin *et al.* prepared PMMA-SiO_2 nanocomposites and studied the drug delivery rate of aspirin. It was observed that the *in vivo* drug release rate of aspirin increased with increase in unmodified silica content, whereas the surface-modified silica in the PMMA composite decreased the drug release rate [122]. Matos *et al.* developed calcium phosphate–PMMA bone cement composites using Mg- and Sr-doped calcium phosphate (CaP) nanoparticles. The CaP nanoparticle was used as a drug carrier of antibiotic delivery systems for the treatment of bone infections such as osteomyelitis. The nanocomposite was studied for the levofloxacin delivery systems and exhibited a sustained release of levofloxacin, with concentrations above the minimum inhibitory concentration values after 48 h [123].

1.5 Fibrous-Nanomaterial-Based Polymer Nanocomposites

The nanofiber-reinforced polymer nanocomposites offer unique properties based on the size and dispersion of fibrous material. The dispersion of the nanofiber and interfacial adhesion at the particle–matrix interface play crucial role in determining the properties of the nanofiber-reinforced polymer. The poor dispersion degrades the physical and mechanical properties of the polymer matrix. A variety of metal, metal oxide, natural, and CFs are used for the preparation of fiber-based polymer nanocomposites.

1.5.1 Natural-Fiber-Reinforced Polymer Nanocomposites

In recent years, natural fibers have received significant attention in the field of polymer composites due to advantages such as reduced tool wear, low cost, low density per unit volume, and acceptable specific strength. The sustainable, renewable, and degradable nature of the natural fibers makes them suitable for use as

nanofillers in polymer composites. A variety of natural fibers such as sisal, jute, wood fibers, and kenaf have been used as fillers in the polymer nanocomposites. Generally, the natural fibers are hydrophilic in nature and possess a comparatively poor fiber/matrix interactions, water resistance, and relatively lower durability [124]. In order to avoid this problem, the surface of the natural fibers needs to be treated with chemical reagents or organic coupling agents. A number of studies have reported the effect of natural fibers on thermal and mechanical properties of polymer nanocomposites [125–130].

1.5.1.1 Mechanical and Thermal Properties of Natural-Fiber-Reinforced Polymer Nanocomposites

Mu *et al.* studied the mechanical properties of sisal fiber/phenol formaldehyde resin generated via *in situ* method and compared the performance with traditional direct mixing composites. It was concluded that the *in situ* composites have better mechanical properties [131]. Arrakhiz *et al.* developed doum fiber-reinforced LDPE composite and studied the effect of incorporation of alkali-treated fiber on the LDPE composites. The authors observed that the addition of 30 wt% fiber increased Young's modulus of LDPE by 145% [132]. Arrakhiz *et al.* studied the influence of chemically treated coir fibers on the mechanical properties of PP. The coir fiber was modified with three reagents, namely silane, sodium hydroxide (NaOH), and dodecane bromide (C12). C12-modified coir fiber increased the Young's modulus of PP by about 120% [133]. Chin and Yousif prepared kenaf fiber reinforcement for tribo–epoxy composites for bearing applications. The authors studied the effect of the fiber orientations, with respect to the sliding direction and the fiber orientations (parallel (P-O), antiparallel (AP-O), and normal (N-O)). It was observed that the presence of kenaf fibers in the composite enhanced the wear and frictional performance of the epoxy and the applied load and sliding velocity had less effect on the specific wear rate of the composite in all the three orientations (Figure 1.7) [134]. Bakar *et al.* studied the thermal and dynamic mechanical properties of grafted-kenaf-filled PVC/ethylene vinyl acetate (EVA) composites. The surface of the kenaf fiber was modified with PMMA. The glass transition temperature (T_g) of the PVC and EVA in the PVC/EVA/kenaf composites was observed to shift to higher temperature with the addition of the kenaf fiber. The crystallinity of the EVA decreased with the addition of 30% grafted and ungrafted kenaf fibers. It was observed that the grafting of PMMA onto the kenaf fibers improved the interaction between the kenaf fiber and PVC/EVA matrix [135]. Paluvai *et al.* studied the mechanical and thermal properties of sisal-fiber-reinforced unsaturated polyester (UP)-toughened epoxy composites. It was reported that the 30 wt% surface modified sisal fibers increased the tensile and flexural strength of unsaturated polyester (UP) resin–epoxy matrix by about 83% and 55%, respectively. Also, the surface-treated fibers and composites exhibited higher thermal stability than the untreated fiber composites [136]. Kakroodi *et al.* derived cellulose nanofibers from *Aloe vera* rind in the form of an aqueous suspension and reinforced into PVA. The addition of nanofibers decreased deformability of PVA significantly and a small amount of (2 wt%) cellulose nanofibers increased

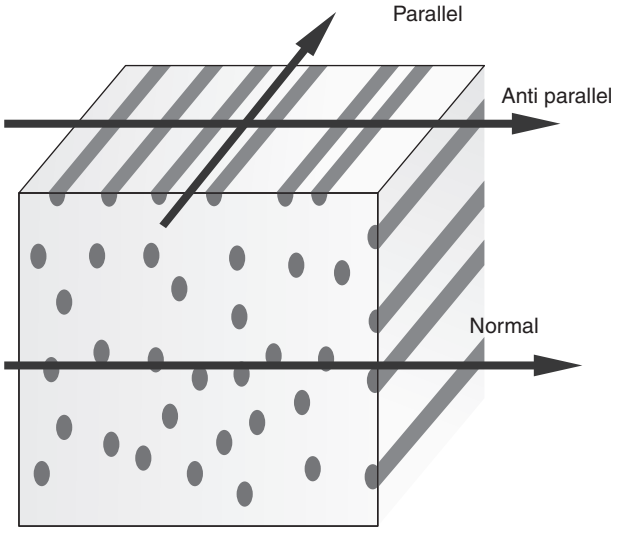

Figure 1.7 Schematic representation of fiber orientations with respect to the sliding direction. (Chin and Yousif [134]. Reproduced with permission of Elsevier.)

the tensile and modulus by 32% and 63%, respectively. They also found that the addition of nanofibers resulted in increased thermal stability of PVA in thermogravimetric analysis due to the reduction in mobility of matrix molecules [137]. George *et al.* studied the thermal, calorimetric, and crystallization behavior of PP/jute yarn biocomposites. The authors observed that the surface-treated jute yarn acted as a nucleating agent and increased the crystallization temperature of the PP due to better interfacial adhesion between jute yarn and PP matrix [138].

1.5.2 Metal and Metal Oxide Fibrous Nanomaterial–Reinforced Polymer Nanocomposites

1-D metal and metal oxide fibrous nanomaterials have been widely used as filler materials for polymer nanocomposites and exhibit good electrical properties due to the higher aspect ratio, leading to lower percolation thresholds.

1.5.2.1 Electrical Properties of Metal and Metal Oxide Nanowire–Reinforced Polymer Nanocomposites

Polymer nanocomposites with high-dielectric-constant (κ) materials have received an increasing interest for various applications including energy storage, high-κ capacitors, electroactive devices, and gate dielectrics [139, 140]. The metal oxide wires such as TiO_2, ZnO, and ZrO_2 possess unique optical and electrical properties, excellent chemical stability, and high dielectric constant properties. The addition of metal oxide nanowires increases the

dielectric constant of the polymer matrix. Xie *et al.* investigated the effect of semiconducting TiO_2 nanowires on electrical properties of epoxy and compared with SiO_2- and TiO_2-nanoparticle-reinforced epoxy nanocomposites. The shape and size of the nanomaterial largely influenced the dielectric properties of the polymer nanocomposites. In fact, 1% loading of TiO_2 nanowires showed higher permittivity values compared with TiO_2 nanoparticles. The authors suggested that the changes in the epoxy nanocomposite system were due to the formation of interface regions caused by nanowire–epoxy interactions and the nature of TiO_2 1-D structure [141]. Tang *et al.* studied the relationship between $BaTiO_3$ nanowire aspect ratio and the dielectric permittivity of PVDF nanocomposites. The authors found that the addition of 30 vol% $BaTiO_3$ nanowires with an aspect ratio of 45.8 enhanced the dielectric constant to 44.3, which was higher (30.7%) than that of polymer nanocomposites containing low aspect ratio of $BaTiO_3$ (9.3) nanowires. It was concluded that the dielectric constant of the nanocomposite increased with the aspect ratio of the nanowires [142].

Metal-reinforced polymer nanocomposites are widely used in the microelectronic applications in the form of conducting material, packaging material, conducting adhesives, and so on. The higher aspect ratio of the 1-D metallic nanowires leads to their electrical carrier nature in one controllable pathway. Thus, increasing the aspect ratio of nanofillers will ultimately increase the conductivity of nanocomposites. This also results in lower percolation thresholds in the conducting polymer nanocomposites [143]. Moreno *et al.* fabricated a transparent conducting polymer nanocomposite film using polycarbonate film with different amounts of Ag nanowires and studied its electrical conductivity. Percolation threshold was observed at very low AgNW content (0.04 wt%), and the composite electrical conductivity at the maximum loading (4.35 wt%) was 41.3 Ω cm [144]. Sureshkumar *et al.* prepared conducting nanocomposites using polystyrene (PS) microspheres and Ag nanowires by latex blending. The Ag nanowire network structure provided electrical pathways to PS monodisperse particles to produce conducting polymer nanocomposites. The incorporation of 0.49 vol% resulted in a percolation threshold, and the addition of 1 vol% resulted in an electrical conductivity of 102 S m^{-1} (Figure 1.8) [145].

There is a possibility for the agglomeration of metal nanowires (MNWs) in the polymer matrix due to their high surface energy. The surface functionalization of MNWs leads to increase in the interfacial adhesion and reduces the agglomeration. Zhao *et al.* developed Ag-nanowire-filled epoxy nanocomposites with amine-modified Ag nanowires. The amine functionalization improved the interfacial adhesion and covalent dispersion of Ag nanowires into the epoxy matrix. Surface resistivity of the AgNW NH_2–epoxy nanocomposite decreased to 1.24×10^5 Ω at 0.5 wt% and the thermal conductivity coefficient was upgraded to 0.67 W m^{-1} K^{-1} at 10 wt% [146]. Luo *et al.* developed conducting LDPE nanocomposites using Ag-coated copper nanowires (AgCuNWs). The nanocomposite contained AgCuNWs of 66.52 wt% and a diameter of 28–33 nm, which exhibited improved antioxidation behavior. It was observed that the addition of

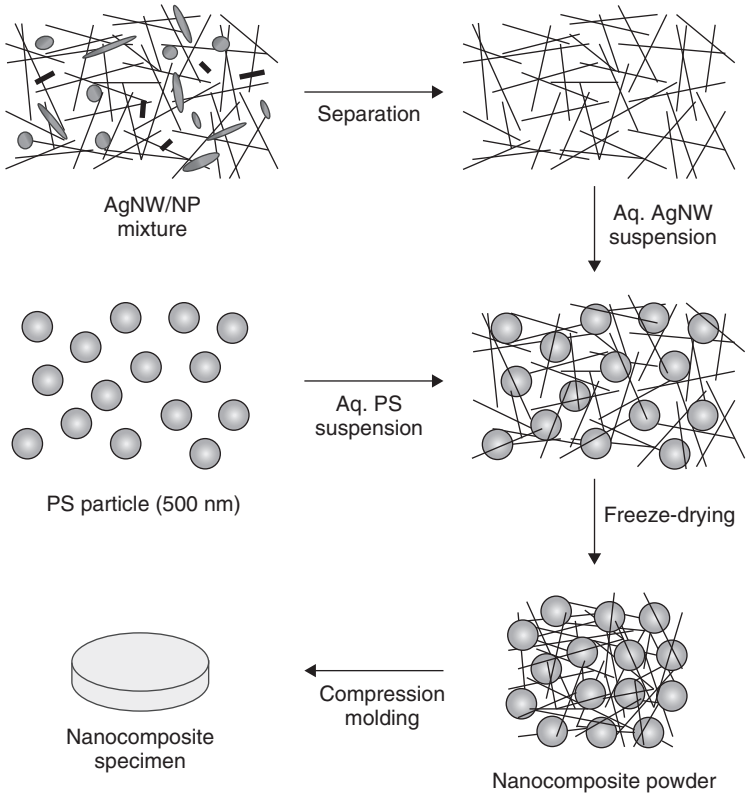

Figure 1.8 Schematic representation of preparation of PS/AgNW nanocomposites with the latex-based process. (Suresh Kumar *et al.* [145]. Reproduced with permission of American Chemical Society.)

AgCuNWs resulted in a less electrical resistivity in LDPE compared to CuNWs in same volume percentage due to the silver content in the AgCuNWs not oxidizing during compression molding [147].

1.5.3 Vapor-Grown Carbon Nanofiber (VGCNF)-Reinforced Polymer Nanocomposites

1-D carbon-based polymer nanocomposites are normally fabricated using single-walled carbon nanotube (SWCNT), multiwalled carbon nanotube (MWCNT), and vapor-grown carbon nanofibers (VGCNFs). Many research studies have focused on CNT-based polymer nanocomposites due to the excellent mechanical properties of nanotubes compared to VGCNFs. However, VGCNFs are low-cost alternatives compared to CNTs and provide better properties especially electrical properties compared to conventional CFs and carbon blacks (CBs) [148].

1.5.3.1 Effect of VGCNFs on Thermal and Mechanical Properties of Polymer Nanocomposites

VGCNFs are promising for the development of polymer nanocomposites due to high thermal stability and mechanical properties. A variety of processing methods such as noncovalent interaction using surfactant grafting and surface functionalization as well as sonication methods have been used for the uniform dispersion of carbon fibrous material in the polymer matrices [149–152]. The surface-treated VGCNFs are observed to be more effective nucleating agents, resulting in higher crystallization temperature and degree of crystallinity compared to nontreated VGCNFs [153]. Lozano and Barrera developed PP/VGNCFs composites and studied isothermal crystallization. It was observed that the addition of 5 wt% CNF led to higher nucleation rates of PP, with an increase in crystallization temperature by 8 °C [154]. Xu *et al.* observed that 3 wt% of surface-functionalized VGNCFs enhanced the thermal conductivity of HDPE by 18% [155]. The addition of VGCNFs strongly influenced the T_g of the polymer nanocomposites. Liu *et al.* found that the addition of the VGCNFs significantly increased the T_g of the polyurethane (PU) nanocomposites as the rigid nanofibers restricted the molecular chain mobility of polymer matrix and resulted in the increment of T_g. [156]. Zhu *et al.* observed that the particle loading and surface functionalization of VGCNFs altered the T_g of the epoxy nanocomposites. The authors observed that the surface-modified VGCNFs increased the T_g of the epoxy nanocomposites by about 10–20 °C compared to unmodified VGCNFs [157]. Adhikari *et al.* studied the fracture toughness of VGCNF-reinforced HDPE nanocomposites. It was observed that the addition of 10 wt% of VGCNFs increased the fracture toughness of HDPE by about 292% [158]. Teng *et al.* grafted polylactide (PLA) on the surface of VGNCFs and reinforced with PLA. The interfacial interaction effectively improved the mechanical properties of PLA nanocomposites. Addition of 10 wt% of PLA-coated VGCNFs enhanced the flexural modulus (to 31.69 N mm^{-2}, increase of 38.6%), flexural strength (101.3 N mm^{-2}, increase of 6.5%), and impact strength (45.98 J m^{-1}, increase of 94%) of the PLA matrix (Figure 1.9) [159]. Yang *et al.* observed a simultaneous increase in both storage (elastic) and loss (viscous dissipation) modulus in aligned VGCNF-reinforced polyethylene nanocomposites [160]. Guo *et al.* observed that the addition of 5 wt% VGNCFs in PAN exhibited an increased tensile modulus and strength of 20% and 50%, respectively [161]

1.5.3.2 Effect of VGCNFs on Electrical Properties of Polymer Nanocomposites

VGCNF-reinforced polymer nanocomposites exhibit improved electrical properties compared to other types of CFs due to larger aspect ratios [162]. Monti *et al.* developed VGCNFs/UP resin nanocomposites and studied their electrical properties. The electrical percolation threshold was observed with the incorporation of 0.3 wt% and the electrical conductivity switched from 10^{-13} to 10^{-7} S cm^{-1} [163]. Ardanuy *et al.* studied the electrical conductivity of epoxy nanocomposites as a function of VGCNFs. The surface conductivity of epoxy nanocomposites increased with increase in loading amount of VGCNFs. The addition of 2 wt%

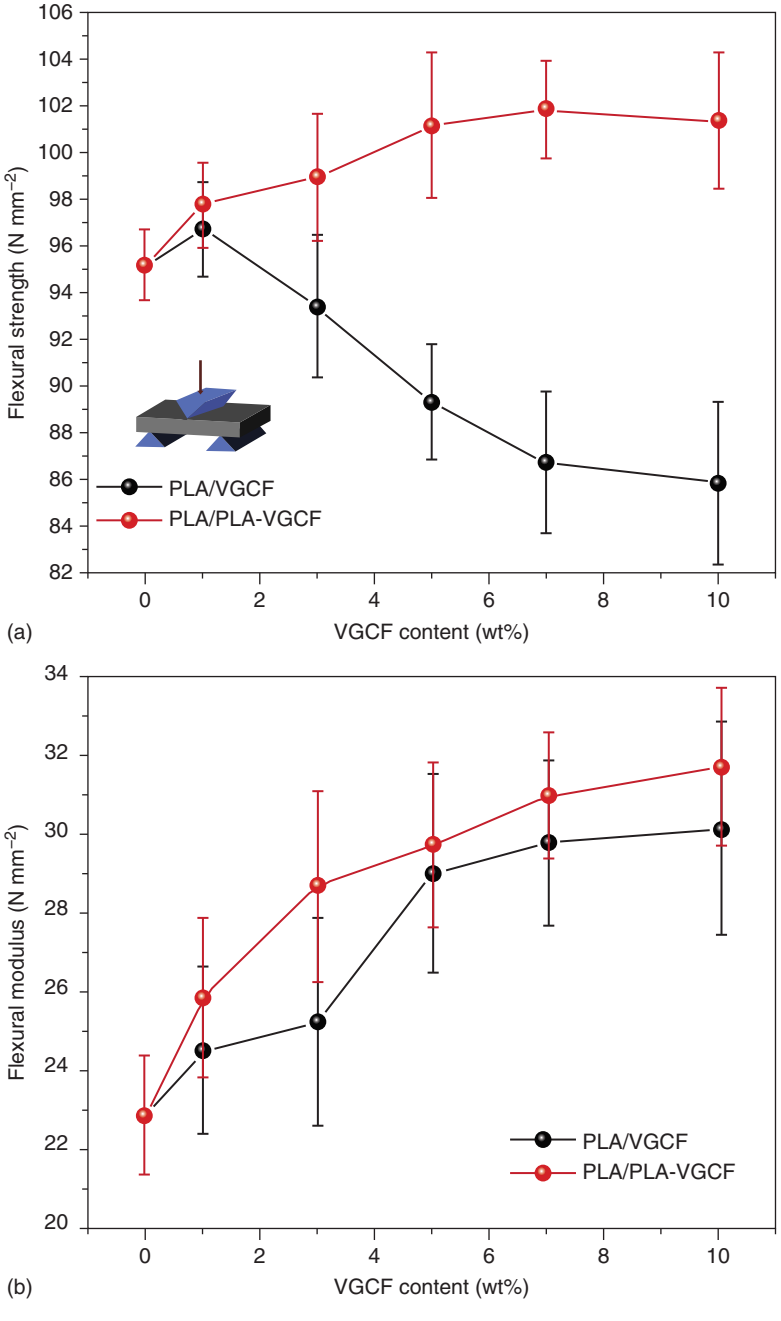

Figure 1.9 (a) Flexural strengths and (b) flexural moduli of PLA nanocomposite incorporating various amounts of pristine VGCF and PLA-VGCF. (Teng *et al.* [159]. Reproduced with permission of Elsevier.)

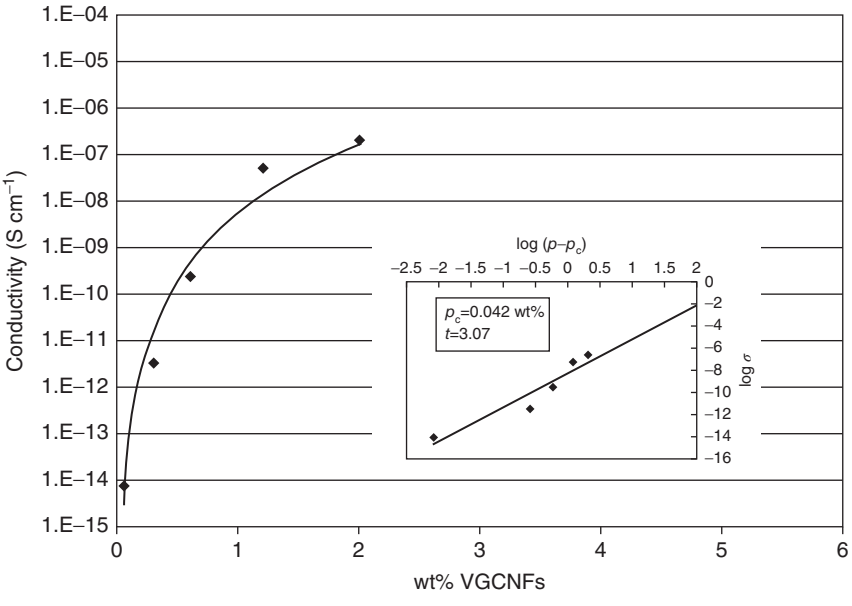

Figure 1.10 Electrical conductivity of epoxy/VGCNFs nanocomposites with respect to VGCNFs content (inset: calculation of the critical exponent by fitting the logarithmic conductivity as a linear function of the logarithmic different between weight percent VGCNF content and critical concentration of VGCNF). (Ardanuy *et al.* [164]. Reproduced with permission of Elsevier.)

VGCNFs exhibited the conductivity of 10^{-6} S cm^{-1}, which was 8 orders of magnitude higher as compared to the pure epoxy matrix (Figure 1.10) [164].

The alignment of VGCNFs significantly influences the electrical properties of polymer nanocomposites. In the polymer nanocomposites, VGCNFs are preferentially aligned parallel to the electric field showing lower electrical resistance and higher dielectric constant [165]. Cardoso *et al.* stated that the dispersion of VGCNFs influenced the electrical conductivity of the epoxy nanocomposites. It was concluded that the homogenous dispersion of the VGCNF did not imply better electrical properties, but the presence of well-distributed nanofiber clusters appeared to be a key factor for increasing composite conductivity [166]. Yang *et al.* studied the dielectric analysis of VGCNF-reinforced polyethylene composites in the frequency range of 0.01 – 105 Hz and temperature range of 35 – 120 °C. It was observed that the dielectric permittivity, loss factor, and tanδ increased with the increase of nanofiber content and decreased with increasing temperature and frequency. Addition of 15 wt% VGCNF exhibited threshold value for permittivity and loss factor in the nanocomposites [167]. Dong *et al.* developed VGCNFs/epoxy shape memory and conductive foams via latex technology. The addition of VGNFs enhanced the strength and electrical conductivity of the epoxy foams. The incorporation of 0.6 wt% of VGCNFs exhibited an electrical percolation threshold in the epoxy nanocomposites [168]. Jiang *et al.* prepared VGCNF-reinforced natural

rubber composites and studied the electrical properties. It was observed that the electrical conductivity and dielectric property of the nanocomposites increased with the increase in nanofiber content. The addition of 4.9 wt% VGCNFs resulted in a percolation threshold in the rubber nanocomposites [169].

1.5.4 Applications of Fibrous-Nanomaterial-Based Polymer Nanocomposites

Fibrous-nanomaterial-based polymer nanocomposites are widely used in the field of aerospace, biomedical, sensors, electromagnetic shielding, radiation resistant, and so on.

1.5.4.1 Biomedical Applications

Biodegradable-polymer-based electrospun nanofibrous scaffolds have gained interest in the tissue engineering field because these mimic the structure of extracellular matrix (ECM) and avoid mechanical mismatch between scaffolds and host tissues [170]. Tissue engineering focuses on the manipulation and regulation of stem cell fate within a hierarchical structure into which cells can attach, spread, differentiate, and increase [171]. Electrospun nanofibers are of commercial importance in vascular, neural, and tendinous tissue engineering [172]. Xiumei *et al.* fabricated poly(L-lactide-*co*-ε-caprolactone) [P(LLACL)] nanofibers and collagen–chitosan complex nanofibers via electrospinning method. It was observed that the biodegradability of P(LLA-CL) nanofibers was faster than its membrane and that smooth muscle cells (SMCs) grew faster on collagen nanofibers than on P(LLA-CL) nanofibers [173]. Chahal *et al.* developed calcium phosphate (CaP)-coated hydroxyl ethyl cellulose (HEC)/PVA nanofibers via electrospinning method. The authors observed that the CaP-coated HEC/PVA scaffolds supported cellular attachment and proliferation of osteosarcoma cells [174]. Recently, researchers have recognized that the electroconducting polymer nanofibers are the promising scaffold material to electrically stimulate neurons and nerve tissues for therapeutic purposes such as nerve tissue engineering scaffolds and neural prostheses [175, 176]. Lee *et al.* fabricated polypyrrole (PPy)-coated electrospun poly(lactic-*co*-glycolic acid) (PLGA) nanofibers and studied the electrical stimulation with a potential of 10 mV cm^{-1} on rat pheochromocytoma 12 (PC12) cells and hippocampal neurons. The PPy-PLGA scaffolds exhibited 40–50% longer neurites and 40–90% more neurite formation compared to unstimulated cells on the same scaffolds (Figure 1.11) [170]. Electrospun nanofibers have been used in drug delivery application as a drug carrier [177]. Li *et al.* prepared PVA-based nanofiber via electrospinning method and used as a drug carrier of caffeine and riboflavin. It was concluded that the PVA/caffeine and PVA/riboflavin nanofibrous mats had almost the same dissolution time (about 1.5 s) and wetting time (about 4.5 s). The release experiments suggested that drugs could be released in a burst manner (caffeine to an extent of 100% and riboflavin to an extent of 40% within 60 s) from the PVA nanofibrous matrices [178]. Lin *et al.* used poly(*N*-isopropyl acrylamide)/poly(caprolactone)-based PU

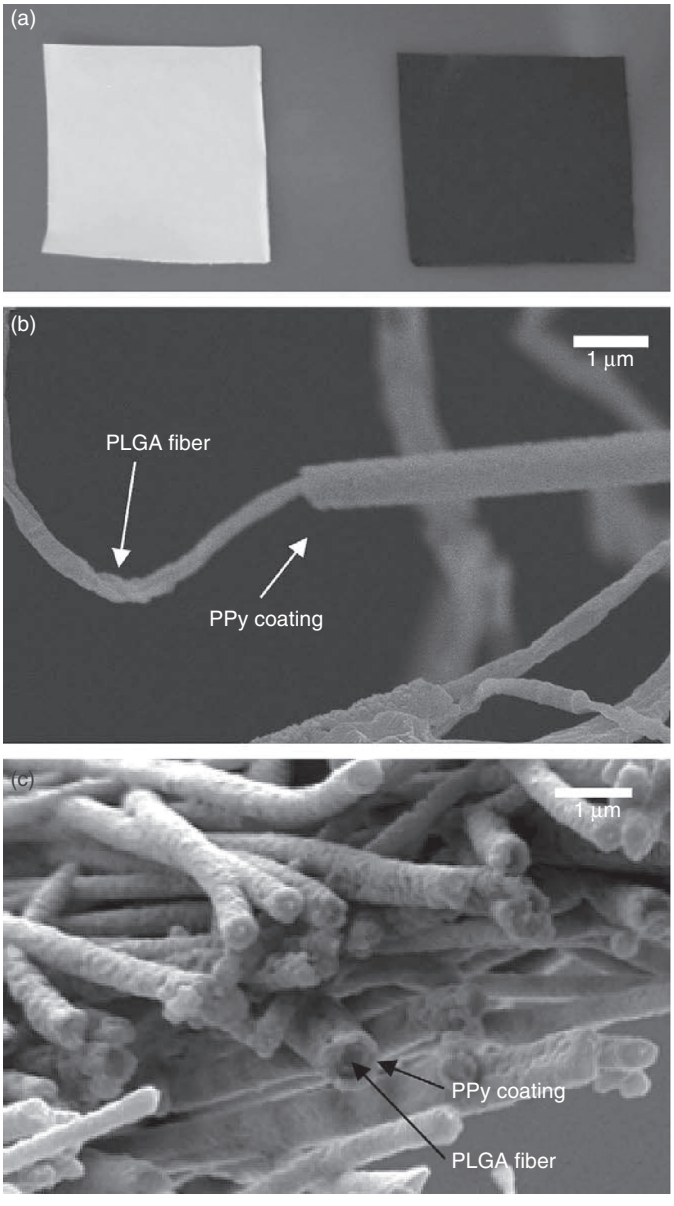

Figure 1.11 PPy-coated PLGA meshes. (a) Photographs of uncoated PLGA meshes (white, left) and PPy-PLGA meshes (black, right). (b) SEM micrograph of single strands of PPy-PLGA fibers. (c) SEM image of section of the PPy-PLGA meshes. (Lee *et al.* [170]. Reproduced with permission of Elsevier.)

nanofibers as drug carriers and studied the temperature-controlled drug release. The nifedipine (NIF) drug was loaded into the nanofibers via cospinning method and the release behavior of NIF could be controlled by the thermo-responsive nanofibers. The release experiments indicated that the release of NIF from the nanofibers could be controlled effectively by adjusting the temperature of the environment surrounding the thermo-responsive nanofibers [179].

1.5.4.2 Electromagnetic Interface (EMI) Shielding Application

Electromagnetic interference (EMI) shielding is defined as the prevention of the propagation of electric and magnetic waves from one region to another by using conducting or magnetic materials. The shielding can be achieved by minimizing the signal passing through a system either by reflection of the wave or by absorption and dissipation of the radiation power inside the material [180]. Conducting polymer nanocomposites are widely used as EMI shielding materials due to lightness, low cost, easy processability, and so on. The 1-D conducting nanomaterials such as metallic nanofibers, carbon-based nanofibers (SWCNT, MWCNT, VGCNFs), and conducting polymer nanofibers have been used as filler materials for the development of polymer nanocomposites in EMI shielding applications due to high aspect ratio. Al-Saleh *et al.* fabricated copper-nanowire-doped PS nanocomposites with high EMI shielding property. In fact, 2.1 vol% of Cu-nanowire-doped PS nanocomposites exhibited an EMI shielding effectiveness (SE) of 35 dB [181]. Yu *et al.* studied the EMI SE of Ag-nanowire-based hydrophilic and hydrophobic nanocomposites and compared these with Cu-nanoparticle-based nanocomposites. The increase in amount of Ag nanowires increased the SE of EMI of the conductive film. Low content of Ag nanowires of nanocomposites showed high shielding efficiency compared to nanoparticle-based nanocomposites, because of the high aspect ratio of the nanowires (Figure 1.12) [182]. Joseph *et al.* prepared polyaniline nanofibers via self-assembling technique and studied the EMI SE property. The authors observed that the nanofibers exhibited an excellent EMI shielding efficiency of about 71–77 dB in the frequency range of 8.2–18 GHz [183].

Carbon-based electrically conductive polymer matrices are most predominant materials for the EMI shielding. Mostly, the 1-D carbon-based conducting polymers have been prepared using SWCNT and MWCNT due to their high aspect ratio. However, the researchers have also used VGCNF as an alternative of CNTs for the development of conducting nanocomposites for EMI shielding study. Nayak *et al.* prepared conducting PI film using different weight ratios of VGCNFs. The authors observed that the loading of 5 wt% VGCNF exhibited EMI SE of above 12 dB in the PI nanocomposites [184]. Yang *et al.* developed the VGCNF-reinforced liquid crystal polymer (LCP) composites and studied the EMI shielding. It was observed that the increase in VGCNF loading in the polymer matrix resulted in an increase in EMI SE in the frequency range of 0.15–1.5 GHz [185]. Zhang *et al.* observed that the thickness of the composite film influenced the shielding effect. The increase in thickness of the composite film increased the EMI SE [186]. Lee *et al.* studied the EMI SE of 40 wt% VGCNF-filled

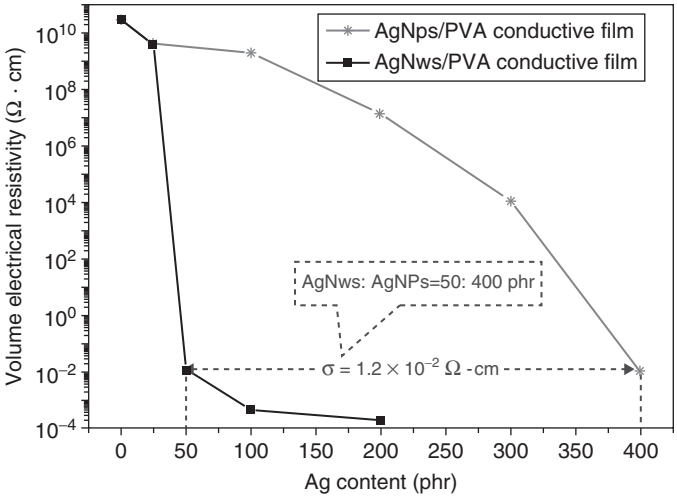

Figure 1.12 Volume electrical resistivity of AgNp and AgNw/epoxy-resin conductive film with various silver contents. (Yu *et al.* [182]. Reproduced with permission of Elsevier.)

PVA nanocomposite and compared with 40% CB-filled PVA nanocomposites. VGCNF-filled PVA film exhibited lower EMI SE compared of CB/PVA film of similar thickness. After heat treatment, the VGCNFs at 1100 °C represented an improved value of EMI SE of the PVA nanocomposite [187].

List of Abbreviations

CO_2	carbon dioxide
CH_4	methane
Co/LiF	cobalt/lithium fluoride
dB	decibel
DC	direct current
EIS	electrochemical impedance spectroscopy
GHz	gigahertz
H_2S	hydrogen sulfide
Hz	hertz
MTS	methyl trichlorosilane
mV	millivolts
Mg	magnesium
PVDF	polyvinylidene fluoride
kV	kilovolt
Sr	strontium
UP resin	unsaturated polyester resin
UV	ultraviolet

References

1. Hayden, T.R. and Pidgeon, N. (2007) Moving engagement 'upstream'? Nanotechnologies and the Royal Society and Royal Academy of Engineering's inquiry. *Public Understanding Sci.*, **16** (3), 345–364.
2. Pomogailo, A. (2006) Synthesis and intercalation chemistry of hybrid organo-inorganic nanocomposites. *Polym. Sci. Ser. C*, **48**, 85–111.
3. Luo, J.J. and Daniel, I.M. (2003) Characterization and modeling of mechanical behavior of polymer/clay nanocomposites. *Compos. Sci. Technol.*, **63**, 1607–1616.
4. McBride, J.R., Dukes, A.D., Schreuder, M.A., and Rosenthal, S.J. (2010) On ultra-small nanocrystals. *Chem. Phys. Lett.*, **498**, 1–3.
5. Harrell, S.M., McBride, J.R., and Rosenthal, S.J. (2013) Synthesis of ultrasmall and magic-sized CdSe nanocrystals. *Chem. Mater.*, **25**, 1199–1210.
6. Kim, B.H., Lee, N., Kim, H., An, K., Park, Y.I., Choi, Y., Shin, K., Lee, Y., Kwon, S.G., Na, H.B., Park, J.G., Ahn, T.Y., Kim, Y.W., Moon, W.K., Choi, S.H., and Hyeon, T. (2011) Large-scale synthesis of uniform and extremely small-sized iron oxide nanoparticles for high-resolution T1 magnetic resonance imaging contrast agents. *J. Am. Chem. Soc.*, **133**, 12624–12631.
7. Bertsch, A., Lorenz, H., and Renaud, P. (1998) Combining micro stereo lithography and thick resist UV lithography for 3D microfabrication. Proceedings of the 11th Annual International Workshop on Micro Electro Mechanical Systems (MEMS 98), pp. 18–23.
8. Alubaidy, A., Venkatakrishnan, K., and Tan, B. (2013) Nanotechnology and nanomaterials, in *Advances in Nanofibers*, Chapter 7, book edited by R. Maguire, ISBN: 978-953-51-1209-9.
9. Liu, H. and Brinson, L.C. (2008) Reinforcing efficiency of nanoparticles: a simple comparison for polymer nanocomposites. *Compos. Sci. Technol.*, **68**, 1502–1512.
10. Kim, B.H., Hackett, M.J., Park, J., and Hyeon, T. (2014) Synthesis, characterization, and application of ultra small nanoparticles. *Chem. Mater.*, **26**, 59–71.
11. Agnihotri, S., Mukherji, S., and Mukherji, S. (2014) Size-controlled silver nanoparticles synthesized over the range 5–100 nm using the same protocol and their antibacterial efficacy. *RSC Adv.*, **4**, 3974–3983.
12. Qian, J.W., Peng, Z.J., Wu, D.Z., and Fu, X.L. (2014) Synthesis and characterization of WO3/S core/shell nanoparticles by thermal evaporation. *Key Eng. Mater.*, **602-603**, 51–54.
13. Kibis, L.S., Stadnichenko, A.I., Pajetnova, E.M., Koscheeva, S.V., Zaykovskii, V.I., and Boronin, A.I. (2010) The investigation of oxidized silver nanoparticles prepared by thermal evaporation and radio-frequency sputtering of metallic silver under oxygen. *Appl. Surf. Sci.*, **257**, 404–413.
14. Li, Y., Peng, R., Xiu, X., Zheng, X., Zhang, X., and Zhai, G. (2011) Growth of SnO_2 nanoparticles via thermal evaporation method. *Superlattices Microstruct.*, **50**, 511–516.
15. Yang, S.M., Kim, S.R.N., Youn, W.K., Kim, C.S., Kim, D.S., Yi, K.W., and Hwang, N.M. (2015) Generation of charged nanoparticles during thermal evaporation of silver at atmospheric pressure. *J. Nanosci. Nanotechnol.*, **15**, 8418–8423.
16. de Carvalho, J.F., de Medeiros, S.N., Morales, M.A., Dantas, A.L., and Carric, A.S. (2013) Synthesis of magnetite nanoparticles by high energy ball milling. *Appl. Surf. Sci.*, **275**, 84–87.
17. Salah, N., Habib, S.S., Khan, Z.H., Memic, A., Azam, A., Alarfaj, E., Zahed, N., and Al-Hamedi, S. (2011) High-energy ball milling technique for ZnO nanoparticles as antibacterial material. *Int. J. Nanomed.*, **6**, 863–869.
18. Munoz, J.E., Cervantes, J., Esparza, R., and Rosas, G. (2007) Iron nanoparticles produced by high-energy ball milling. *J. Nanopart. Res.*, **9**, 945–950.

19. Pingali, K.C., Rockstraw, D.A., and Deng, S. (2005) Silver nanoparticles from ultrasonic spray pyrolysis of aqueous silver nitrate. *Aerosol Sci. Technol.*, **39**, 1010–1014.
20. Wang, W.N., Itoh, Y., Lenggoro, I.W., and Okuyama, K. (2004) Nickel and nickel oxide nanoparticles prepared from nickel nitrate hexahydrate by a low pressure spray pyrolysis. *Mater. Sci. Eng., B*, **111**, 69–76.
21. Wang, W.N., Lenggoro, I.W., Terashi, Y., Kim, T.O., and Okuyama, K. (2005) One-step synthesis of titanium oxide nanoparticles by spray pyrolysis of organic precursors. *Mater. Sci. Eng., B*, **123**, 194–202.
22. Darroudi, M., Sabouri, Z., Oskuee, R.K., Zake, A.K., Kargar, H., and Hamid, M.H.N.A. (2013) Sol–gel synthesis, characterization, and neurotoxicity effect of zinc oxide nanoparticles using gum tragacanth. *Ceram. Int.*, **39**, 9195–9199.
23. Tabatabaei, S., Shukohfar, A., Aghababazadeh, R., and Mirhabibi, A. (2006) Experimental study of the synthesis and characterisation of silica nanoparticles via the sol-gel method. *J. Phys. Conf. Ser.*, **26**, 371–374.
24. Lu, Y., Yin, Y., Mayers, B.T., and Xia, Y. (2002) Modifying the surface properties of superparamagnetic iron oxide nanoparticles through a Sol – Gel approach. *Nano Lett.*, **2**, 183–186.
25. Moharram, A.H., Mansour, S.A., Hussein, M.A., and Rashad, M. (2014) Direct precipitation and characterization of ZnO nanoparticles. *J. Nanomater.*, 5 pp., Article ID 716210.
26. Bala, H., Fu, W., Zhao, J., Ding, X., Jiang, Y., Yu, K., and Wang, Z. (2005) Preparation of BaSO4 nanoparticles with self-dispersing properties. *Colloids Surf., A*, **252**, 129–134.
27. Wang, B., Huang, X., Zhu, Z., Huang, H., and Dai, J. (2012) Hydrothermal synthesis method of nickel phosphide nanoparticles. *Appl. Nanosci.*, **2**, 423–427.
28. Ge, S., Shi, X., Sun, K., Li, C., Uher, C., Baker, J.R., Mark, J.M., Holl, B., and Orr, B.G. (2009) Facile hydrothermal synthesis of iron oxide nanoparticles with tunable magnetic properties. *J. Phys. Chem. C*, **113**, 13593–13599.
29. Takami, S., Sato, T., Mousavand, T., Ohara, S., Umetsu, M., and Adschir, T. (2007) Hydrothermal synthesis of surface-modified iron oxide nanoparticles. *Mater. Lett.*, **61**, 4769–4772.
30. Rosemary, M.J. and Pradeep, T. (2003) Solvothermal synthesis of silver nanoparticles from thiolates. *J. Colloid Interface Sci.*, **268**, 81–84.
31. Bai, X., Li, L., Liu, H., Tan, L., Liu, T., and Meng, X. (2015) Solvothermal synthesis of ZnO nanoparticles and anti-infection application in vivo. *ACS Appl. Mater. Interfaces*, **7**, 1308–1317.
32. Lian, J., Liang, Y., Kwong, F.L., Ding, Z., and Ng, D.H.L. (2012) Template-free solvothermal synthesis of ZnO nanoparticles with controllable size and their size-dependent optical properties. *Mater. Lett.*, **66**, 318–320.
33. Gan, H., Li, Y., Liu, H., Wang, S., Li, C., Yuan, M., Liu, X., Wang, C., Jiang, L., and Zhu, D. (2007) Self-assembly of conjugated polymers and ds-oligonucleotides directed fractal-like aggregates. *Biomacromolecules*, **8**, 1723–1729.
34. Jian, X., Weijun, L., Honglai, L., and Ying, H. (2007) Controlled synthesis of uniform silver nanowires with high aspect ratios in aqueous solutions of gemini surfactant. *Front. Chem. Eng. China*, **1**, 221–227.
35. Song, Y., Garcia, R.M., Dorin, R.M., Wang, H., Qiu, Y., Coker, E.N., Steen, W.A., Miller, J.E., and Shelnutt, J.A. (2007) Synthesis of platinum nanowire networks using a soft template. *Nano Lett.*, **7**, 3650–3655.
36. Chang, M.H., Cho, H.A., Kim, Y.S., Lee, E.J., and Kim, J.Y. (2014) Thin and long silver nanowires self-assembled in ionic liquids as a soft template: electrical and optical properties. *Nanoscale Res. Lett.*, **9**, 330.
37. Zhou, Q., Chen, W., Xu, L., and Peng, S. (2013) Hydrothermal synthesis of various hierarchical ZnO nanostructures and their methane sensing properties. *Sensors*, **13**, 6171–6182.

38. Charbonneau, C., Gauvin, R., and Demopoulos, G.P. (2009) Nucleation and growth of self-assembled nanofibre-structured rutile (TiO_2) particles via controlled forced hydrolysis of titanium tetrachloride solution.. *J. Cryst. Growth*, **31**, 86–94.
39. Dong, W.S., Lin, F.Q., Liu, C.L., and Li, M.Y. (2009) Synthesis of ZrO_2nanowires by ionic-liquid route. *J. Colloid Interface Sci.*, **333**, 734–740.
40. Pal, J., Sanwaria, S., Srivastava, R., Nandan, B., Horechyy, A., Stamm, M., and Chen, H.L. (2012) Hairy polymer nanofibers via self-assembly of block copolymers. *J. Mater. Chem.*, **22**, 25102–25107.
41. Fu, J., Huang, X., Zhu, Y., Huang, Y., Zhu, L., and Tang, X. (2008) Rapid fabrication and formation mechanism of cyclotriphosphazene-containing polymer nanofibers. *Eur. Polym. J.*, **44**, 3466–3472.
42. Neyts, E., Maeyens, A., Pourtois, G., and Bogaerts, A. (2011) A density-functional theory simulation of the formation of Ni-doped fullerenes by ion implantation. *Carbon*, **49**, 1013–1017.
43. Gazit, E. (2007) Use of biomolecular templates for the fabrication of metal nanowires. *FEBS J.*, **274**, 317–322.
44. Toe, W.E. and Ramakrishna, S. (2006) A review on electrospinning design and nanofibre assemblies. *Nanotechnology*, **17**, R89–R106.
45. Shao, C., Kim, H.Y., Gong, J., Ding, B., Lee, D.R., and Park, S.J. (2003) Fiber mats of poly(vinyl alcohol)/silica composite via electrospinning. *Mater. Lett.*, **57**, 1579–1584.
46. Dong, Z.Q., Ma, X.H., Xu, Z.L., and Gu, Z.Y. (2015) Superhydrophobic modification of PVDF–SiO_2 electrospun nanofiber membranes for vacuum membrane distillation. *RSC Adv.*, **5**, 67962.
47. Bae, H.S., Haider, A., Selim, K.M.K., Kang, D.Y., Kim, E.J., and Kang, I.-K. (2013) Fabrication of highly porous PMMA electrospun fibers and their application in the removal of phenol and iodine. *J. Polym. Res.*, **20**, 158.
48. Gu, S.Y., Ren, J., and Wu, Q.L. (2005) Preparation and structures of electrospun PAN nanofibers as a precursor of carbon nanofibers. *Synth. Met.*, **155**, 157–161.
49. Zhou, Z., Lai, C., Zhang, L., Qian, Y., Hou, H., Reneker, D.H., and Fong, H. (2009) Development of carbon nanofibers from aligned electrospun polyacrylonitrile nanofiber bundles and characterization of their microstructural, electrical, and mechanical properties. *Polymer*, **50**, 2999–3006.
50. Park, J.Y., Choi, S.W., and Kim, S.S. (2010) A synthesis and sensing application of hollow ZnO nanofibers with uniform wall thicknesses grown using polymer templates. *Nanotechnology*, **21**, 475601 (9pp).
51. Liu, M., Cheng, Z., Yan, J., Qiang, L., Ru, X., Liu, F., Ding, D., and Li, J. (2013) Preparation and characterization of TiO_2 nanofibers via using polylactic acid as template. *J. Appl. Polym. Sci.*, **128**, 1095–1100.
52. Wu, H., Hu, L., Rowell, M.W., Kong, D., Cha, J.J., McDonough, J.R., Zhu, J., Yang, Y., McGehee, M.D., and Cui, Y. (2010) Electrospun metal nanofiber webs as high-performance transparent electrode. *Nano Lett.*, **10**, 4242–4248.
53. Gries, K., Vieker, H., Gölzhäuser, A., Agarwal, S., and Greiner, A. (2012) Preparation of continuous gold nanowires by electrospinning of high-concentration aqueous dispersions of gold nanoparticles. *Small*, **8**, 1436–1441.
54. Yi, G.C., Wang, C., and Park, W.I. (2005) ZnO nanorods: synthesis, characterization and applications. *Semicond. Sci. Technol.*, **20**, S22–S34.
55. Chang, P.C., Fan, Z., Wang, D., Tseng, W.Y., Chiou, W.A., Hong, J., and Lu, J.G. (2004) ZnO nanowires synthesized by vapor trapping CVD method. *Chem. Mater.*, **16**, 5133–5137.
56. Manafi, S.A. and Badiee, S.H. (2008) Production of carbon nanofibers using a CVD method with lithium fluoride as a supported cobalt catalyst. *Res. Lett. Mater. Sci.*, 5 pp., Article ID 850975.
57. Fu, Q.G., Li, H.J., Shi, X.H., Li, K.Z., Wei, J., and Hu, Z.B. (2006) Synthesis

of silicon carbide nanowires by CVD without using a metallic catalyst. *Mater. Chem. Phys.*, **100**, 108–111.

58. Dai, Z.R., Pan, Z.W., and Wang, Z.L. (2003) Novel nanostructures of functional oxides synthesized by thermal evaporation. *Adv. Funct. Mater.*, **13**, 9–24.
59. Wu, J.M., Shih, H.C., Wu, W.T., Tseng, Y.K., and Chen, I.C. (2005) Thermal evaporation growth and the luminescence property of TiO_2 nanowires. *J. Cryst. Growth*, **281**, 384–390.
60. Li, S.Y., Lee, C.Y., Lin, P., and Tseng, T.Y. (2005) Low temperature synthesized Sn doped indium oxide nanowires. *Nanotechnology*, **16**, 451–457.
61. Bae, S.Y., Na, C.W., Kang, J.H., and Park, J. (2005) Comparative structure and optical properties of Ga-, In-, and Sn-doped ZnO nanowires synthesized via thermal evaporation. *J. Phys. Chem. B*, **109**, 2526–2531.
62. Noda, T., Suzuki, H., Araki, H., Yang, W., Shi, Y., and Tosa, M. (2005) Microstructures and IR spectra of long amorphous SiO_2/Si nanowires. *Appl. Surf. Sci.*, **241**, 231–235.
63. Sen, S., Xie, Y., Kumar, S.K., Yang, H., Bansal, A., Ho, D.L., Hall, L., Hooper, J.B., and Schweizer, K.S. (2007) Chain conformations and bound-layer correlations in polymer nanocomposites. *Phys. Rev. Lett.*, **98**, 128302.
64. Jouault, N., Dalmas, F., Said, S., Di Cola, E., Schweins, R., Jestin, J., and Boue, F. (2010) Direct measurement of polymer chain conformation in well-controlled model nanocomposites by combining SANS and SAXS. *Macromolecules*, **43**, 9881–9891.
65. Mackay, M.E., Tuteja, A., Duxbury, P.M., Hawker, C.J., Van Horn, B., Guan, Z., Chen, G.H., and Krishnan, R.S. (2006) General strategies for nanoparticle dispersion. *Science*, **311**, 1740–1743.
66. Karatrantos, A., Clarke, N., Composto, R.J., and Winey, K.I. (2015) Polymer conformations in polymer nanocomposites containing spherical nanoparticles. *Soft Matter*, **11**, 382–388.
67. Karatrantos, A., Clarke, N., Composto, R.J., and Winey, K.I. (2014) Structure, entanglements and dynamics of polymer nanocomposites containing spherical nanoparticles. *IOP Conf. Ser. Mater. Sci. Eng.*, **64**, 012041.
68. Vengatesan, M.R. and Mittal, V. (2015) Surface modification of nanomaterials for application in polymer nanocomposites: an overview, in *Surface Modification of Nanoparticle and Natural Fiber Fillers* (ed V. Mittal), Wiley-VCH Verlag GmbH & Co. KGaA, Weinheim, doi: 10.1002/9783527670260.ch1.
69. Šupová, M., Martynková, G.S., and Barabaszová, K. (2011) Effect of nanofillers dispersion in polymer matrices: a review. *Sci. Adv. Mater.*, **3**, 1–25.
70. Hamming, L.M., Qiao, R., Messersmith, P.B., and Brinson, L.C. (2009) Effects of dispersion and interfacial modification on the macroscale properties of TiO_2 polymer–matrix nanocomposites. *Compos. Sci. Technol.*, **69**, 1880–1886.
71. Mandhakini, M., Lakshmikandhan, T., Chandramohan, A., and Alagar, M. (2014) Effect of nanoalumina on the tribology performance of C4-ether-linked bismaleimide-toughened epoxy nanocomposites. *Tribol. Lett.*, **54**, 67–79.
72. Rajamanikam, R., Pichaimani, P., Kumar, M., and Muthukaruppan, A. (2015) Optical and thermomechanical behavior of benzoxazine functionalized ZnO reinforced polybenzoxazine nanocomposites. *Polym. Compos.* doi: 10.1002/pc.23758
73. Avella, M., Cosco, S., Di Lorenzo, M.L., Di Pace, E., Errico, M.E., and Gentile, G. (2006) Nucleation activity of nanosized $CaCO_3$ on crystallization of isotactic polypropylene, in dependence on crystal modification, particle shape, and coating. *Eur. Polym. J.*, **42**, 1548–1557.
74. Zhang, Z., Tao, Y., Yang, Z., and Mai, K. (2008) Preparation and characteristics of nano-$CaCO_3$ supported b-nucleating agent of polypropylene. *Eur. Polym. J.*, **44**, 1955–1961.
75. Farhoodi, M., Mousavi, S.M.A., Gharebagh, R.S., Djomeh, Z.E., and

Oromiehie, A. (2014) Preparation and characteristics of nano-$CaCO_3$ supported b-nucleating agent of polypropylene. *J. Thermoplast. Compos. Mater.*, **27**, 1127–1138.

76. Yu, W., Lan, C.H., Wang, S.J., Fang, P.F., and Sun, Y.M. (2010) Influence of zinc oxide nanoparticles on the crystallization behavior of electrospun poly(3-hydroxybutyrate-co-3-hydroxyvalerate) nanofibers. *Polymer*, **51**, 2403–2409.

77. Gómez, M., Bracho, D., Palza, H., and Quijada, R. (2015) Effect of morphology on the permeability, mechanical and thermal properties of polypropylene/SiO_2 nanocomposites. *Polym. Int.*, **64**, 1245–1251.

78. Jin, H.Y., Yang, Y.Q., Xu, L., and Hou, S.E. (2011) Effects of spherical silica on the properties of an epoxy resin system. *J. Appl. Polym. Sci.*, **121**, 648–653.

79. Isitman, N.A., Dogan, M., Bayramli, E., and Kaynak, C. (2012) The role of nanoparticle geometry in flame retardancy of polylactide nanocomposites containing aluminium phosphinate. *Polym. Degrad. Stab.*, **97**, 1285–1296.

80. Fu, S.Y., Feng, X.Q., Lauke, B., and Mai, Y.W. (2008) Effects of particle size, particle/matrix interface adhesion and particle loading on mechanical properties of particulate–polymer composites. *Composites Part B*, **39**, 933–961.

81. Katz, H.S. and Mileski, J.V. (1987) *Handbook of Fillers for Plastics*, 2nd edn, Van Nostrand Reinhold Co., New York, pp. 119–142.

82. Lin, Y., Chen, H., Chan, C.M., and Wu, J. (2008) High impact toughness polypropylene/$CaCO_3$ nanocomposites and the toughening mechanism. *Macromolecules*, **41**, 9204–9213.

83. Fu, Q., Wang, G., and Sen, J. (1993) Polyethylene toughened by CaCO3 particle: brittle-ductile transition of CaCO3-toughened HDPE. *J. Appl. Polym. Sci.*, **49**, 673–677.

84. Fu, Q. and Wang, G. (1993) Effect of morphology on brittle-ductile transition of HPDE/$CaCO_3$ blends. *J. Appl. Polym. Sci.*, **49**, 1985–1988.

85. Fu, Q. and Wang, G. (1993) Polyethylene toughened by caco3 particles—percolation model of brittle-ductile transition in HDPE/$CaCO_3$ blends. *Polym. Int.*, **30**, 309–312.

86. Hussain, M., Nakahira, A., Nishijima, S., and Niihara, K. (1996) Effects of coupling agents on the mechanical properties improvement of the TiO_2 reinforced epoxy system. *Mater. Lett.*, **26**, 299–303.

87. Yoshida, Y., Higashihara, T., Nomura, Y., Usui, E., and Hibi, S. (1999) The effect of silane agent on tensile and bending properties of silica-filled epoxy after water absorption by boiling. *Electr. Eng. Jpn.*, **129**, 1–12.

88. Ash, B.J., Siegel, R.W., and Schadler, L.S. (2004) Mechanical behavior of alumina/poly(methyl methacrylate) nanocomposites. *Macromolecules*, **37**, 1358–1369.

89. Jeziórska, R., Świerz-Motysia, B., Zielecka, M., Szadkowska, A., and Studziński, M. (2012) Structure and mechanical properties of low-density polyethylene/spherical silica nanocomposites prepared by melt mixing: the joint action of silica's size, functionality, and compatibilizer. *J. Appl. Polym. Sci.*, **125**, 4326–4337.

90. Rao, J.K., Raizada, A., Ganguly, D., Mankad, M.M., Satyanarayana, S.V., and Madhu, G.M. (2015) Enhanced mechanical properties of polyvinyl alcohol composite films containing copper oxide nanoparticles as filler. *Polym. Bull.* doi: 10.1007/s00289-015-1386-4

91. Rithin Kumar, N.B., Crasta, V., Bhajantri, R.F., and Praveen, B.M. (2014) Microstructural and mechanical studies of PVA doped with ZnO and WO_3 composites films. *J. Polym.*, 7 pp., Article ID 846140.

92. Salehian, H. and Jahromi, S.A.J. (2014) Effect of titanium dioxide nanoparticles on mechanical properties of vinyl ester-based nanocomposites. *J. Compos. Mater.* doi: 10.1177/0021998314546140

93. Liawthanyarat, N. and Rimdusit, S. (2015) Effects of particles size of nanosilica on properties of polybenzoxazine nanocomposites. *Key Eng. Mater.*, **659**, 394–398.

94. Basu, R. and Iannacchione, G.S. (2008) Dielectric response of multiwalled carbon nanotubes as a function of applied ac-electric fields. *J. Appl. Phys.*, **104**, 114107.
95. Dang, Z., Shen, Y., Fan, L., Cai, N., Nan, C., and Zhao, S. (2003) Dielectric properties of carbon fiber filled low-density polyethylene. *J. Appl. Phys.*, **93**, 5543.
96. Guo, Q., Zhu, P., Li, G., Huang, L., Zhang, Y., Lu, D.D., Sun, R., and Wong, C. (2015) One-pot synthesis of bimodal silica nanospheres and their effects on the rheological and thermal–mechanical properties of silica–epoxy composites. *RSC Adv.*, **5**, 50073–50081.
97. Zhaa, J.W., Danga, Z.M., Zhoub, T., Song, H.T., and Chen, G. (2010) Electrical properties of TiO_2-filled polyimide nanocomposite films prepared via an in situ polymerization process. *Synth. Met.*, **160**, 2670–2674.
98. Tuncer, E., Sauers, I., James, D.R., Ellis, A.R., Paranthaman, M.P., Aytuğ, T., Sathyamurthy, S., More, K.L., Li, J., and Goyal, A. (2007) Electrical properties of epoxy resin based nano-composites. *Nanotechnology*, **18**, 025703 (6pp).
99. Jiang, K., Cheng, L., Zheng, L., Yao, Z., Li, G., and Yin, Q. (2007) The unique dielectric behaviour of nanosilica epoxy composites. Proceedings of the 7th IEEE International Conference on Nanotechnology, Hong Kong, August 2–5, 2007.
100. Yang, T.I., Brown, R.N.C., Kempel, L.C., and Kofinas, P. (2008) Magneto-dielectric properties of polymer–Fe_3O_4 nanocomposites. *J. Magn. Magn. Mater.*, **320**, 2714–2720.
101. Chandrakala, H.N., Ramaraj, B., Shivakumaraiah, Madhu, G.M., and Siddaramaiah (2012) The influence of zinc oxide–cerium oxide nanoparticles on the structural characteristics and electrical properties of polyvinyl alcohol films. *J. Mater. Sci.*, **47**, 8076–8084.
102. Hong, J.I., Schadler, L.S., and Siegel, R.W. (2003) Rescaled electrical properties of ZnO/low density polyethylene nanocomposites. *Appl. Phys. Lett.*, **82**, 1956.
103. Goyal, R.K. and Sulakhe, R. (2015) Study on poly (vinylidene fluoride)/nickel composites with low percolation. *Adv. Mater. Lett.*, **6**, 309–317.
104. Mahendia, S., Tomar, A.K., and Kumar, S. (2010) Electrical conductivity and dielectric spectroscopic studies of PVA–Ag nanocomposite films. *J. Alloys Compd.*, **508**, 406–411.
105. Tee, D.I., Mariatti, M., Azizan, A., See, C.H., and Chong, K.F. (2007) Effect of silane-based coupling agent on the properties of silver nanoparticles filled epoxy composites. *Compos. Sci. Technol.*, **67**, 2584–2591.
106. Macyk, W., Szaciłowski, K., Stochel, G., Buchalsk, M., Kuncewicza, J., and Łabuz, P. (2010) Titanium(IV) complexes as direct TiO_2 photosensitizers. *Coord. Chem. Rev.*, **254**, 2687–2701.
107. Paz, Y. (2010) Application of TiO_2 photo catalysis for air treatment: patents' overview. *Appl. Catal., B*, **99**, 448–460.
108. Su, W., Wang, S., Wang, X., Fu, X., and Weng, J. (2010) Plasma pre-treatment and TiO_2 coating of PMMA for the improvement of antibacterial properties. *Surf. Coat. Technol.*, **205**, 465–469.
109. Shaik, M.R., Alam, M., and Alandis, N.M. (2015) Development of castor oil based poly (urethane-esteramide)/TiO_2 nanocomposites as anticorrosive and antimicrobial coatings. *J. Nanomater.*, 10 pp., Article ID 745217.
110. Wang, N., Fu, W., Zhang, J., Li, X., and Fang, Q. (2015) Corrosion performance of waterborne epoxy coatings containing polyethylenimine treated mesoporous-TiO_2 nanoparticles on mild steel. *Prog. Org. Coat.*, **89**, 114–122.
111. Olad, A. and Nosrati, R. (2013) Preparation and corrosion resistance of nanostructured PVC/ZnO–polyaniline hybrid coating. *Prog. Org. Coat.*, **76**, 113–118.
112. Ghanbari, A. and Attar, M.M. (2015) A study on the anticorrosion performance of epoxy nanocomposite coatings containing epoxy-silane treated nano-silica on mild steel substrate. *J. Ind. Eng. Chem.*, **23**, 145–153.

113. Arsuaga, J.M., Sotto, A., Rosario, G., Martínez, A., Molina, S., Teli, S.B., and Abajo, J. (2013) Influence of the type, size, and distribution of metal oxide particles on the properties of nanocomposite ultrafiltration membranes. *J. Membr. Sci.*, **428**, 131–141.

114. Zhao, S., Yan, W., Shi, M., Wang, Z., Wang, J., and Wang, S. (2015) Improving permeability and antifouling performance of polyethersulfone ultrafiltration membrane by incorporation of ZnO-DMF dispersion containing nano-ZnO and polyvinylpyrrolidone. *J. Membr. Sci.*, **478**, 105–116.

115. Huang, J., Zhang, K., Wang, K., Xie, Z., Ladewig, B., and Wang, H. (2012) Fabrication of polyethersulfone-mesoporous silica nanocomposite ultra-filtration membranes with antifouling properties. *J. Membr. Sci.*, **423–424**, 362–370.

116. Sotto, A., Boromand, A., Balta, S., Kim, J., and Bruggen, B.V. (2011) Doping of polyethersulfone nanofiltration membranes: antifouling effect observed at ultralow concentrations of TiO_2 nanoparticles. *J. Mater. Chem.*, **21**, 10311–10320.

117. Maximous, N., Nakhla, G., Wan, W., and Wong, K. (2009) Preparation, characterization and performance of Al_2O_3/PES membrane for wastewater filtration. *J. Membr. Sci.*, **341**, 67–75.

118. Nour, M., Berean, K., Chrimes, A., Zoolfakar, A.S., Latham, K., Sweeney, C.M., Field, M.R., Sriram, S., Kalantar-zadeh, K., and Ou, J.Z. (2014) Silver nanoparticle/PDMS nanocomposite catalytic membranes for H_2S gas removal. *J. Membr. Sci.*, **470**, 346–355.

119. Daniels, A.U., Chang, M.K.O., Andriano, K.P., and Heller, J. (1990) Mechanical properties of biodegradable polymers and composites proposed for internal fixation of bone. *J. Appl. Biomater.*, **1**, 57–78.

120. Shameli, K., Ahmad, M.B., Yunus, W.M.Z.W., Ibrahim, N.A., Rahman, R.A., Jokar, M., and Darroudi, M. (2010) Silver/poly (lactic acid) nanocomposites: preparation, characterization, and antibacterial activity. *Int. J. Nanomed.*, **5**, 573–579.

121. Carlo, G.D., Curulli, A., Toro, R.G., Bianchini, C., Caro, T.D., Padeletti, G., Zane, D., and Ingo, G.M. (2012) Green synthesis of gold–chitosan nanocomposites for caffeic acid sensing. *Langmuir*, **28**, 5471–5479.

122. Lin, M., Wang, H., Meng, S., Zhong, W., Li, Z., Cai, R., Chen, Z., Zhou, X., and Du, Q. (2007) Structure and release behavior of PMMA/silica composite drug delivery system. *J. Pharm. Sci.*, **96**, 1518–1526.

123. Matos, A.C., Marques, C.F., Pinto, R.V., Ribeiro, I.A.C., Gonçalves, L.M., Vaz, M.A., Ferreira, J.M.F., Almeida, A.J., and Bettencourt, A.F. (2015) Novel doped calcium phosphate-PMMA bone cement composites as levofloxacin delivery systems. *Int. J. Pharm.*, **490**, 200–208.

124. Saba, N., Tahir, P.M., and Jawaid, M. (2014) A review on potentiality of nano filler/natural fiber filled polymer hybrid composites. *Polymers*, **6**, 2247–2273.

125. Ku, H., Wang, H., Pattarachaiyakoop, N., and Trada, M. (2011) A review on the tensile properties of natural fiber reinforced polymer composites. *Composites Part B*, **42**, 856–873.

126. Boopalan, M., Umapathy, M.J., and Jenyfer, P. (2012) A comparative study on the mechanical properties of jute and sisal fiber reinforced polymer composites. *Silicon*, **4**, 145–149.

127. Sapuan, S.M., Leenie, A., Harimi, M., and Beng, Y.K. (2006) Mechanical properties of woven banana fibre reinforced epoxy composites. *Mater. Des.*, **27**, 689–693.

128. Kuboki, T., Lee, Y.H., Park, C.B., and Sain, M. (2009) Mechanical properties and foaming behavior of cellulose fiber reinforced high-density polyethylene composites. *Polym. Eng. Sci.*, **49**, 2179–2188.

129. Karmarkar, A., Chauhan, S.S., Modak, J.M., and Chanda, M. (2007) Mechanical properties of wood–fiber reinforced polypropylene composites: effect of a novel compatibilizer with isocyanate functional group. *Composites Part A*, **38**, 227–233.

130. Mohammed, L., Ansari, M.N.M., Pua, G., Jawaid, M., and Islam, M.S. (2015)

A review on natural fiber reinforced polymer composite and its applications. *Int. J. Polym. Sci.*, 15 pp., Article ID 243947.

131. Mu, Q., Wei, C., and Feng, S. (2009) Studies on mechanical properties of sisal fiber/phenol formaldehyde resin in-situ composites. *Polym. Compos.*, **30**, 131–137.
132. Arrakhiz, F.Z., Achaby, M.E., Malha, M., Bensalah, M.O., Fehri, O.F., Bouhfid, R., Benmoussa, K., and Qaiss, A. (2013) Mechanical and thermal properties of natural fibers reinforced polymer composites: Doum/low density polyethylene. *Mater. Des.*, **43**, 200–205.
133. Arrakhiz, F.Z., Achaby, M.E., Kakou, A.C., Vaudreuil, S., Benmoussa, K., Bouhfid, R., Fassi-Fehri, O., and Qaiss, A. (2012) Mechanical properties of high density polyethylene reinforced with chemically modified coir fibers: impact of chemical treatments. *Mater. Des.*, **37**, 379–383.
134. Chin, C.W. and Yousif, B.F. (2009) Potential of kenaf fibres as reinforcement for tribological applications. *Wear*, **267**, 1550–1557.
135. Bakar, N.A., Chee, C.Y., Abdullah, L.C., Ratnam, C.T., and Ibrahim, N.A. (2015) Thermal and dynamic mechanical properties of grafted kenaf filled poly (vinyl chloride)/ethylene vinyl acetate composites. *Mater. Des.*, **65**, 204–211.
136. Paluvai, N.R., Mohanty, S., and Nayak, S.K. (2015) Unsaturated polyester-toughened epoxy composites: effect of sisal fiber on thermal and dynamic mechanical properties. *J. Vinyl Add. Technol.* doi: 10.1002/vnl.21491
137. Kakroodi, A.R., Cheng, S., Sain, M., and Asiri, A. (2014) Mechanical, thermal, and morphological properties of nanocomposites based on polyvinyl alcohol and cellulose nanofiber from *Aloe vera* rind. *J. Nanomater.*, 7 pp., Article ID 903498.
138. George, G., Joseph, K., Nagarajan, E.R., Jose, E.T., and Skrifvars, M. (2013) Thermal, calorimetric and crystallisation behaviour of polypropylene/jute yarn bio-composites fabricated by commingling technique. *Composites Part A*, **48**, 110–120.
139. Li, Y., Huang, X., Hu, Z., Jiang, P., Li, S., and Tanaka, T. (2011) Large dielectric constant and high thermal conductivity in poly(vinylidene fluoride)/barium titanate/silicon carbide three-phase nanocomposites. *ACS Appl. Mater. Interfaces*, **3**, 4396–4403.
140. Zirkl, M., Haase, A., Fian, A., Schön, H., Sommer, C., Jakopic, G., Leising, G., Stadlober, B., Graz, I., Gaar, N., Schwödiauer, R., Bauer-Gogonea, S., and Bauer, S. (2007) Low-voltage organic thin-film transistors with high-k nanocomposite gate dielectrics for flexible electronics and optothermal sensors. *Adv. Mater.*, **19**, 2241–2245.
141. Xie, Q., Niu, C.M., and Cheng, Y.H. (2015) Preparation and electrical properties of titania nanowire-epoxy nanocomposites. Electrical Insulation Conference (EIC), Seattle, WA, June 7–10, 2015.
142. Tang, H., Zhou, Z., and Sodano, H.A. (2014) Relationship between BaTiO3 nanowire aspect ratio and the dielectric permittivity of nanocomposites. *ACS Appl. Mater. Interfaces*, **6**, 5450–5455.
143. Murphy, C.J. and Jana, N.R. (2002) Controlling the aspect ratio of inorganic nanorods and nanowires. *Adv. Mater.*, **14**, 80–82.
144. Moreno, I., Navascues, N., Arruebo, M., Irusta, S., and Santamaria, J. (2013) Facile preparation of transparent and conductive polymer films based on silver nanowire/polycarbonate nanocomposites. *Nanotechnology*, **24**, 275603 (11pp).
145. Sureshkumar, M., Na, H.Y., Ahn, K.H., and Lee, S.J. (2015) Conductive nanocomposites based on polystyrene microspheres and silver nanowires by latex blending. *ACS Appl. Mater. Interfaces*, **7**, 756–764.
146. Zhao, T., Zhang, C., Du, Z., Li, H., and Zou, W. (2015) Functionalization of AgNWs with amino groups and their application in an epoxy matrix for antistatic and thermally conductive nanocomposites. *RSC Adv.*, **5**, 91516–91523.
147. Luo, X., Gelves, G.A., Sundararaj, U., and Luo, J.-L. (2013) Silver-coated

copper nanowires with improved anti-oxidation property as conductive fillers in low-density polyethylene. *Can. J. Chem. Eng.*, **91**, 630–637.

148. Saleh, M.H.A. and Sundararaj, U. (2009) A review of vapor grown carbon nanofiber/polymer conductive composites. *Carbon*, **47**, 2–22.
149. Gong, X., Liu, J., Baskaran, S., Voise, R.D., and Young, J.S. (2000) Surfactant-assisted processing of carbon nanotube/polymer composites. *Chem. Mater.*, **12**, 1049–1052.
150. Hill, D.E., Lin, Y., Rao, A.M., Allard, L.F., and Sun, Y.P. (2002) Functionalization of carbon nanotubes with polystyrene. *Macromolecules*, **35**, 9466–9471.
151. Lin, Y., Zhou, B., Fernando, K.A.S., Liu, P., Allard, L.F., and Sun, Y.P. (2003) Polymeric carbon nanocomposites from carbon nanotubes functionalized with matrix polymer. *Macromolecules*, **36**, 7199–7204.
152. Park, C., Ounaies, Z., Watson, K.A., Crooks, R.E., Smith, J. Jr., Lowther, S.E., Connell, J.W., Siochi, E.J., Harrison, J.S., and Clair, T.L.S. (2002) Dispersion of single wall carbon nanotubes by in situ polymerization under sonication. *Chem. Phys. Lett.*, **364**, 303–308.
153. Lee, S., Hahn, J.R., Ku, B.C., and Kim, J. (2011) Effect of carbon nanofiber structure on crystallization kinetics of polypropylene/carbon nanofiber composites. *Bull. Korean Chem. Soc.*, **32**, 2369–2376.
154. Lozano, K. and Barrera, E.V. (2001) Nanofiber-reinforced thermoplastic composites. I. Thermoanalytical and mechanical analyses. *J. Appl. Polym. Sci.*, **79**, 125–133.
155. Xu, S., Akchurin, A., Liu, T., Wood, W., Tangpong, X.W., Akhatov, I.S., and Zhong, W.H. (2014) Thermal properties of carbon nanofiber reinforced high-density polyethylene nanocomposites. *J. Compos. Mater.* doi: 10.1177/0021998314525980
156. Liu, W., Xu, K., Wang, C., Qian, B., Sun, Y., Zhang, Y., Xie, H., and Cheng, R. (2015) Carbon nanofibers reinforced soy polyol-based polyurethane nanocomposites. *J. Therm. Anal. Calorim.* doi: 10.1007/s10973-015-4690-1
157. Zhu, J., Wei, S., Ryu, J., Budhathoki, M., Liang, G., and Guo, Z. (2010) In situ stabilized carbon nanofiber (CNF) reinforced epoxy nanocomposites. *J. Mater. Chem.*, **20**, 4937–4948.
158. Adhikari, A.R., Partida, E., Petty, T.W., Jones, R., Lozano, K., and Guerrero, C. (2009) Fracture toughness of vapor grown carbon nanofiber-reinforced polyethylene composites. *J. Nanomater.*, 6 p, Article ID 101870.
159. Teng, C.C., Maa, C.C.M., Cheng, B.D., Shih, Y.F., Chen, J.W., and Hsiao, Y.K. (2011) Mechanical and thermal properties of polylactide-grafted vapor-grown carbon nanofiber/polylactide nanocomposites. *Composites Part A*, **42**, 928–934.
160. Yang, S., Tijerina, J.T., Diaz, V.S., Hernandez, K., and Lozano, K. (2007) Dynamic mechanical and thermal analysis of aligned vapor grown carbon nanofiber reinforced polyethylene. *Composites Part B*, **38**, 228–235.
161. Guo, H., Rasheed, A., Minus, M.L., and Kumar, S. (2008) Polyacrylonitrile/vapor grown carbon nanofiber composite films. *J. Mater. Sci.*, **43**, 4363–4369.
162. Xu, J., Donohoe, J.P., and Pittman, C.U. Jr., (2004) Preparation, electrical and mechanical properties of vapor grown carbon fiber (VGCF)/vinyl ester composites. *Composites Part A*, **35**, 693–701.
163. Monti, M., Terenzi, A., Natali, M., Gaztelumendi, I., Markaide, N., Kenny, J.M., and Torre, L. (2010) Development of unsaturated polyester matrix – carbon nanofibers nanocomposites with improved electrical properties. *J. Appl. Polym. Sci.*, **117**, 1658–1666.
164. Ardanuy, M., Rodríguez-Perez, M.A., and Algaba, I. (2011) Electrical conductivity and mechanical properties of vapor-grown carbon nanofibers/trifunctional epoxy composites prepared by direct mixing. *Composites Part B*, **42**, 675–681.
165. Simoes, R., Silva, J., Mendez, S.L., and Vaia, R. (2010) Influence of fiber

aspect ratio and orientation on the dielectric properties of polymer-based nanocomposites. *J. Mater. Sci.*, **45**, 268–270.

166. Cardoso, P., Silva, J., Klosterman, D., Covas, J.A., Hattum, F.W.J., Simoes, R., and Mendez, S.L. (2011) The influence of the dispersion method on the electrical properties of vapor-grown carbon nanofiber/epoxy composites. *Nanoscale Res. Lett.*, **6**, 370, (5pages).

167. Yang, S., Benitez, R., Fuentes, A., and Lozano, K. (2007) Dielectric analysis of VGCNF reinforced polyethylene composites. *Compos. Sci. Technol.*, **67**, 1159–1166.

168. Dong, Y., Ding, J., Wang, J., Fu, X., Hu, H., Li, S., Yang, H., Xu, C., Du, M., and Fu, Y. (2013) Synthesis and properties of the vapour-grown carbon nanofiber/epoxy shape memory and conductive foams prepared via latex technology. *Compos. Sci. Technol.*, **76**, 8–13.

169. Jiang, H., Ni, Q., and Wang, H. (2013) Preparation and electrical property evaluation of vapor-grown carbon nanofibers reinforced natural rubber composites. *J. Ind. Text.*, **42**, 340–350.

170. Lee, J.Y., Bashur, C.A., Goldstein, A.S., and Schmidt, C.E. (2009) Polypyrrole-coated electrospun PLGA nanofibers for neural tissue applications. *Biomaterials*, **30**, 4325–4335.

171. Huebsch, N. and Mooney, D.J. (2009) Inspiration and application in the evolution of biomaterials. *Nature*, **26**, 426–432.

172. Srouji, S., Kizhner, T., Tobi, E.S., Livne, E., and Zussman, E. (2008) 3-D nanofibrous electrospun multilayered construct is an alternative ECM mimicking scaffold. *J. Mater. Sci. Mater. Med.*, **19**, 1249–1255.

173. Xiumei, M., Zonggang, C., and Weber, H.J. (2007) Electrospun nanofibers of collagen-chitosan and P(LLA-CL) for tissue engineering. *Front. Mater. Sci. Chin.*, **1**, 20–23.

174. Chahal, S., Hussain, F.S.J., Kumar, A., Yusoffa, M.M., and Rasad, M.S.B.A. (2015) Electrospun hydroxyethyl cellulose nanofibers functionalized with calcium phosphate coating for bone tissue engineering. *RSC Adv.*, **5**, 29497–29504.

175. Guimard, N.K., Gomez, N., and Schmidt, C.E. (2007) Conducting polymers in biomedical engineering. *Prog. Polym. Sci.*, **32**, 876–921.

176. Ateh, D.D., Navsaria, H.A., and Vadgama, P. (2006) Polypyrrole-based conducting polymers and interactions with biological tissues. *J. R. Soc. Interface*, **3**, 741–752.

177. Hu, X., Liu, S., Zhou, G., Huang, Y., Xie, Z., and Jing, X. (2014) Electrospinning of polymeric nanofibers for drug delivery applications. *J. Controlled Release*, **185**, 12–21.

178. Li, X., Kanjwal, M.A., Lind, L., and Chronakis, I.S. (2013) Electrospun polyvinyl-alcohol nanofibers as oral fast-dissolving delivery system of caffeine and riboflavin. *Colloids Surf., B*, **103**, 182–188.

179. Lin, X., Tang, D., Gu, S., Dua, H., and Jiang, E. (2013) Electro spun poly (N-isopropyl acrylamide)/poly (caprolactone)-based polyurethane nanofibers as drug carriers and temperature-controlled release. *New J. Chem.*, **37**, 2433–2439.

180. Thomassin, J.M., Jérôme, C., Pardoen, T., Bailly, C., Huynen, I., and Detrembleur, C. (2013) Polymer/carbon based composites as electromagnetic interference (EMI) shielding materials. *Mater. Sci. Eng., R*, **74**, 211–232.

181. Saleh, M.H.A., Gelves, G.A., and Sundararaj, U. (2011) Copper nanowire/polystyrene nanocomposites: lower percolation threshold and higher EMI shielding. *Composites Part A*, **42**, 92–97.

182. Yu, Y.H., Ma, C.C.M., Teng, C.C., Huang, Y.L., Lee, S.H., Wang, I., and Wei, M.H. (2012) Electrical, morphological, and electromagnetic interference shielding properties of silver nanowires and nanoparticles conductive composites. *Mater. Chem. Phys.*, **136**, 334–340.

183. Joseph, N., Varghese, J., and Sebastian, M.T. (2015) Self-assembled polyaniline

nanofibers with enhanced electromagnetic shielding properties. *RSC Adv.*, **5**, 20459–20466.

184. Nayak, L., Chaki, T.K., and Khastgir, D. (2014) Electrical percolation behavior and electromagnetic shielding effectiveness of polyimide nanocomposites filled with carbon nanofibers. *J. Appl. Polym. Sci.*, **131**, 40914.

185. Yang, S., Lozano, K., Lomeli, A., Foltz, H.D., and Jones, R. (2005) Electromagnetic interference shielding effectiveness of carbon nanofiber/LCP composites. *Composites Part A*, **36**, 691–697.

186. Zhang, C.S., Ni, Q.Q., Fu, S.Y., and Kurashiki, K. (2007) Electromagnetic interference shielding effect of nanocomposites with carbon nanotube and shape memory polymer. *Compos. Sci. Technol.*, **67**, 2973–2980.

187. Lee, B.O., Woo, W.J., and Kim, M.-S. (2001) EMI shielding effectiveness of carbon nanofiber filled poly (vinyl alcohol) coating materials. *Macromol. Mater. Eng.*, **286**, 114–118.